Modeling transport phenomena with COMSOL Multiphysics

Adsorptive membrane fouling in lignocellulosic biorefineries and lessons learned from it

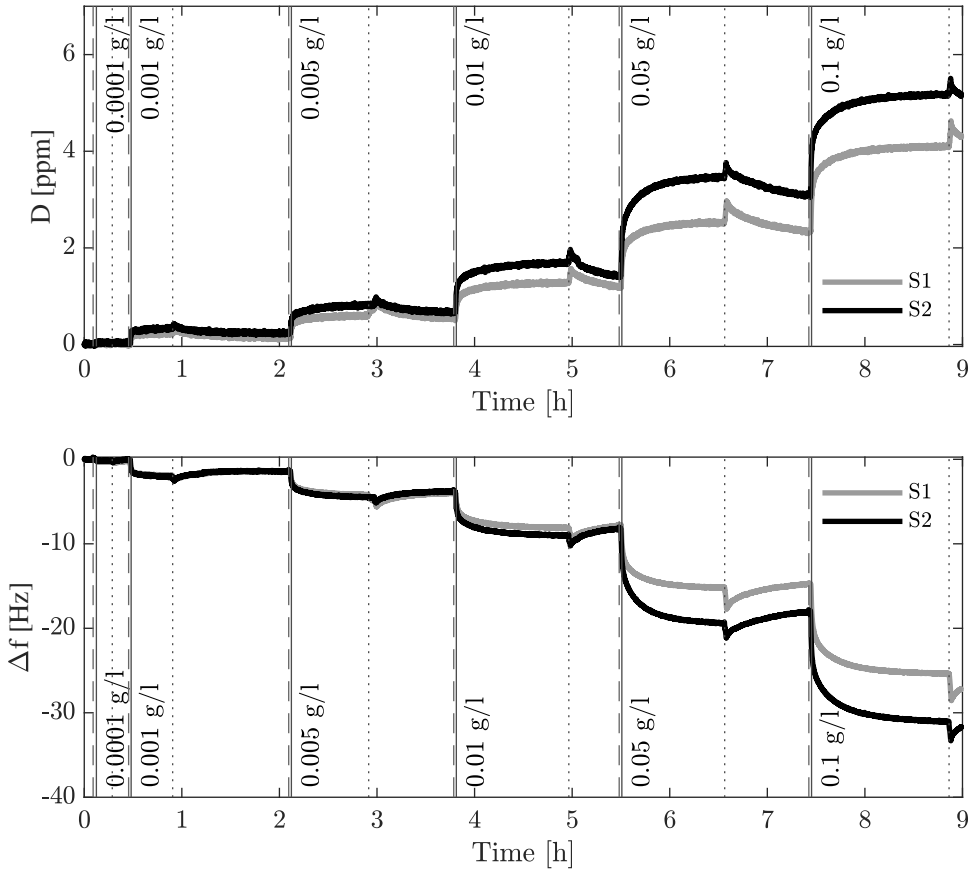

Linnéa Petersson

Department of Chemical Engineering
Master Thesis 2020

LUND UNIVERSITY

LUND UNIVERSITY

Master Thesis

Modeling transport phenomena with COMSOL Multiphysics

Adsorptive membrane fouling in lignocellulosic biorefineries and lessons learned from it

by

Linnéa Petersson

Department of Chemical Engineering
Lund University
Sweden

2020

Supervisors: **Gregor Rudolph & Anton Löfgren**
Examiner: **Frank Lipnizki**

Postal address
PO-Box 124
SE-221 00 Lund, Sweden

Visiting address
Naturvetarvägen 14

Telephone
+46 46-222 82 85
+46 46-222 00 00

Web address
www.lth.se/chemeng

Printed in Sweden by Media-Tryck.
Lund 2020

Acknowledgement

There are many people i want to thank for making this project possible and bearable.

First I want to thank my supervisors Gregor Rudolph and Anton Lövgren for for your support, time and answers to my never-ending questions and to professor Frank Lipnizki for being the examiner.

Second, a thank you to the department of physical chemistry and professor Tommy Nylander for the opportunity to use the QCM-D equipment.

Third, I want to thank all the nice people at the department of chemical engineering for your support. You made the freezing offices of Kemicentrum feel a lot warmer and welcoming.

Fourth, I want to thank my mother Vivian, my father Bo and my sister Alicia for always supporting me, and especially for the 15 portions of homecooked meals that sustained me in the weeks leading up to the presentation of this thesis.

Last, I want to thank all the friends I made at the Chemical Engineering and Biotechnology programs. The past five years wouldn't have been half as fun without you and I wouldn't have learned half as much either.

Thank You!

Abstract

The separation of hemicelluloses, like glactoglucomannans, from lignocellulosic process streams is an important step in building profitable lignocellulosic biorefineries. The most common method for the separation is membrane filtration, however, it has the draw-back of being sensitive to membrane fouling. To better understand the fouling process, it is desirable to be able to model the adsorption of hemicelluloses onto the membrane surface, since adsorption is a contributing mechanism in fouling.

In this project, a model was developed in COMSOL Multiphysics® v.5.3. to simulate the adsorption of glucose, dextran and GGM as model compounds onto a model membrane surface of polysulfone and one of gold, respectively. The model in COMSOL considered bulk fluid dynamics and adsorption kinetics. The adsorption kinetics was investigated using Quartz crystal microbalance with dissipation monitoring (QCM-D). Glucose and dextran had too weak adsorption kinetics to develop a suitable adsorption model. The adsorption of GGM was best described with pseudo-second-order model, compared with a pseudo-first-order model and the Langmuir adsorption model.

The pseudo-second-order model was unsuccessfully integrated with the COMSOL model as it lacked a direct connection to the bulk concentration. A reference model based on literature data for Langmuir kinetics failed to produce results comparable with the literature data. Further investigations into the adsorption kinetics for adsorption of hemicelluloses are needed to build a computer model for membrane fouling. These investigations need to consider the validity of the adsorption kinetic models applied as well as the underlying assumptions of the experimental methods.

Popular Science Summary

Att försöka simulera adsorption

av Linnéa Petersson

Datormodeller är användbara för att förutspå verkligheten men bara om man lyckas få dem att återspegla den först. För adsorptionsfenomen är detta extra knepigt då det är många underliggande antaganden som måste identifieras och uppfyllas.

Att kunna testa hypoteser i en datormodell innan man testar den i labbet eller ute i en stor fabrik är något som kan spara både tid och resurser. Ett område där en datormodell kan vara intressant är när man studerar nedsmutsning av membran, så kallad membranfouling. Membran används idag för att separera olika ämnen från processströmmar baserat på ämnenas storlek. Vissa ämnen går igenom membranen, medan andra hålls kvar. Problemet är att ämnena också kan smutsa ner membranen genom att fastna på och i membranen vilket gör att de fungerar sämre. En typ av membranfouling sker genom adsorption, vilket är när ämnena på molekylnivå fäster sig på materialet som membranet är uppbyggt av.

För att kunna beskriva adsorption på membran med en datormodell behöver man veta två saker; 1. Hur rör sig ämnena i flödet när de inte sitter fast på membranytan? 2. Hur ser adsorptionskinetiken ut? Det vill säga: Hur snabbt fastnar ämnena på ytan och kan de lossna igen?

Den första frågan är relativt lätt att besvara då det finns många färdigbyggda datorprogram som beskriver hur olika ämnen rör sig med ett flöde och det finns mycket litteratur om hur ämnen rör sig genom ett flöde, till exempel av vatten. Man kan på så sätt få datorprogrammet att beskriva vilken koncentration som finns av ett ämne i varje punkt i flödet och hur den här koncentrationen förändras med tiden.

Den andra frågan är svårare då adsorptionskinetiken är specifik för kombinationen av ämne och material på ytan som ämnet fastnar på. Det finns olika typer av uttryck för att beskriva adsorptionskinetik där var och en har egna underliggande antaganden som måste uppfyllas för att uttrycket ska återspegla verkligheten. Det mest kända uttrycket för adsorptionskinetik är Langmuirkinetik som bland annat kräver att ämnet som adsorberar på ytan endast bygger upp ett lager som är en molekyl tjockt. För att kunna bestämma adsorptionskinetiken behöver man också göra experiment där man mäter hur mycket av ämnet som fäster på ytan beroende på koncentrationen man hade från början. Det finns många metoder för detta varav en metod är Quartz Crystal Microbalance and Dissipation Monitoring (QCM-D) som utnyttjar att frekvensen på vibrationerna i en kvartskristall som utsätts för ett elektriskt fält ändras när kristallens massa ökar, till exempel genom att något adsorberar på dess yta.

När man har besvarat de två frågorna och byggt ihop det till en datormodell finns det ytterligare en fråga man måste ställa sig. Återspeglar min modell verkligheten? I detta fall blev svaret nej. De viktigaste orsakerna till detta var att de underliggande antagandena för de undersökta adsorptionskinetiken samt för användandet av QCM-D inte var helt uppfyllda. När detta sker finns det bara en sak att göra, lära sig av sina misstag och försöka igen.

Contents

List of symbols & abbreviation

Symbols

C	Mass sensitivity constant	ng/(cm^2 Hz)
c_A	Bulk concentration	mol/L, mol/m^3
c_s	Concentration of adsorbed substance on surface	mol/m^2
D	Dissipation	ppm
D_A	Diffusivity	m^2/s
D_s	Surface diffusivity	m^2/s
k_{ads}	Adsorption coefficient Langmuir	L/(mols), 1/(wt%s)
k_{des}	Desorption coefficient Langmuir	1/s
k_0	Decay constant	1/s
k_1	Adsorption rate constant pseudo-first-order	1/s
k_2	Adsorption rate constant pseudo-second-order	m^2/(s mol)
n	Overtone number	3,5,7...
q_t	Adsorption capacity at time t pseudo-order models	mol/m^2
q_e	Adsorption capacity at equilibrium pseudo-order models	mol/m^2
r	Adsorption rate	mol/(m^2 s)
Δf	Frequency shift	Hz
Δf_{eq}	Frequency shift at equilibrium	Hz
Δm_f	Adsorbed mass per surface area	ng/cm^2
Γ_s	Maximum concentration of adsorption sites Langmuir	mol/m^2
θ	Fractional surface coverage	-
θ	Surface coverage at equilibrium	-

Abbreviations

DP	Degree of polymerisation
GGM	Galactoglucomannans
PEO	Polyethylene oxide
PNIPAM	poly(*N*isopropylacrylamide)
PSU	Polysulfone
QCM-D	Quartz crystal microbalance with dissipation monitoring

1 Introduction

1.1 Overview

The forest industry is an important cornerstone in the Swedish economy. It is the third-largest exporter of forest products and the fourth largest exporter of pulp and paper worldwide (Sörensson and Jonsson, 2014). Still, the forest industry is facing challenges such as increasing global competition, restricted environmental laws and decreasing demand on pulp and paper due to the shift from newsprint to electronic media (Bokhary et al., 2017). To improve revenue, more and more pulp and paper mills are being re-purposed to lignocellulosic biorefineries. While a pulp and paper mill mainly uses the cellulose to make pulp and paper biorefineries strive to utilise lignin, hemicellulose and extractives from the wood and turn them into products such as value-added chemicals or biofuels.

A key challenge for using process matter from lignocellulosic biorefineries is the recovery of the components as they are present in low concentration in the process water (Thuvander, Lipnizki, and A.-S. Jönsson, 2019) and are sensitive to degradation (Bokhary et al., 2017). Membrane technologies have proven themselves to be the most promising option to perform these separations efficiently, with low energy cost and without degrading the components (Bokhary et al., 2017). The drawback with membrane technologies is that the membranes are prone to fouling, which reduces performance and shortens the membrane lifespan.

To better understand the membrane fouling mechanisms, the build-up of fouling on a model surface can be studied using quartz crystal microbalance with dissipation monitoring (QCM-D). QCM-D provides a close-to real-time insight into the development of fouling on a model layer of the membrane surface over time. If the development of fouling over time is better understood, it can be used to optimise the operating conditions to limit the formation of fouling.

A digital twin of a QCM-D cell to simulate the adsorption phenomena would provide a way to qualitatively predict the results of QCM-D before performing experiments.

1.2 Aim

The aim of this thesis project is to model the adsorption processes of hemicelluloses on a model membrane surface. For this, a QCM-D cell will be modelled in COMSOL Multiphysics® v.5.3. A simulation of a reference system based on literature data will be done to test the applicability of the simulation. Adsorption parameters are determined by QCM-D experiments.

2 Theory

2.1 Biorefineries & Membranes

In Sweden, the key raw material for lignocellulosic biorefineries and pulp mills is wood. The components in wood can be divided into four main categories: cellulose, hemicellulose, lignin and extractives (Schmitt, Koch, and Lehnen, 2014). Woods can be divided into softwoods, for example spruce and fir, and hardwoods, for example birch and maple, depending on the ratio of the components. Cellulose makes up 40 % to 44 % of the wood. It forms long, unbranched chains of D-glucose, usually with a degree of polymerisation between 70 000 and 15 000. Hemicelluloses consist of several kinds of sugars, are branched and have a degree of polymerisation of 50 to 200. Softwoods contain 25 % to 30 % hemicellulose while hardwoods contain 30 % to 35 %. Lignin is an irregular structure of cross-linked polyphenols and makes out 25 % to 32 % of softwoods and 18 % to 25 % in hardwoods. Extractives are a group of compounds with low molecular mass and make up 1 % to 5 % of the woods common in Europe. Hydrophobic extractives, like terpenes, phenols, fats and waxes, can be extracted with organic solvents while hydrophilic extractives, like tannins and inorganic salts, can be extracted with hot water.

Pulping of wood means that the wood is processed to create a suspension of its fibres (Ragnar et al., 2014). The pulp can then be further processed to create paper, board or rayon and other cellulose derivatives. The pulping can either be a chemical process, like the Kraft process, or a mechanical process, like thermomechanical pulping. The different processes yield pulp with different properties, mostly due to the lignin content in the final pulp.

Membrane plants in lignocellulosic biorefineries and pulp mills need several stages to properly separate the different fractions in the process streams (A.-S. Jönsson, 2013). First particles and fibres have to be removed through either filtration or centrifugation then the process stream can be treated using a combination of pressure-driven membrane processes like microfiltration (MF), ultrafiltration (UF)

and nanofiltration (NF). Microfiltration can remove suspended solids and colloids, but has low retention of lignin. MF membranes can retain compounds from 10 µm down to 0.1 µm and are operated at less than 2 bar. Ultrafiltration can remove macromolecules such as lignin and hemicellulose. UF membranes retain compounds from 20 nm down to 1 nm and operate at pressures from 2 bar to 10 bar. Nanofiltration (NF) removes sugars and has membranes with smaller pores than UF but larger pores than the membranes used to separate salts from water through reverse osmosis. The fractionation using MF, UF and NF can also be complemented with diafiltration to increase purity of the retentate and reverse osmosis to remove ions to produce high-quality water.

Membrane processes for separation and recovery of lignocellulosic compounds have several advantages(A.-S. Jönsson, 2013). They have a low energy requirement and chemical consumption and the need to adjust the pH or the temperature of the process stream can be mitigated by the choice of membrane material. They are also able to separate the products with very little degradation (Bokhary et al., 2017). However, the main drawback of membrane processes is that they are prone to fouling(A.-S. Jönsson, 2013). Membrane fouling is visible as a reduction of flux at constant operating pressure that can not be reversed by changing the operating condition. To restore a fouled membrane, cleaning or membrane replacement is required. The main mechanisms of membrane fouling are cake layer formation, pore blocking and adsorption on the pore walls. Larger solutes that are retained by the membrane cause cake layer formation and pore blocking on the membrane surface. Smaller solutes can adsorb on the pore walls within the membrane and reduce the effective pore diameter. The different fouling phenomena requires different countermeasures, such as back-pulsing for cake layer formation, reduced poor size for pore blocking and more hydrophilic membrane or change of pH for adsorption.

2.1.1 Polysulfone membranes

A commonly used type of membranes for UF in biorefineries are polysulfone (PSU) membranes (Persson et al., 2010; Al-Rudainy, Galbe, and Wallberg, 2017; Dal-Cin et al., 1996). PSU is a hydrophobic membrane polymer but can be modified to increase the hydrophilicity (Tremblay, Tam, and Guiver, 1992; Ding et al., 2016). Commercially available hydrophilic PSU membranes are the FX5-pHt and UFX10-pHt membranes (Alfa Laval, 2020). Other types of membranes are polyvinylidenefouride, polyacrylonitrile, polyether-imide, cellulosic membranes (Dal-Cin et al., 1996).

2.1.2 Galactoglucomannans

Galactoglucomannans (GGM) are polysaccharides and the most common type of hemicelluloses in softwood, making out 15-23 % of the mass (Schmitt, Koch, and Lehnen, 2014). Their availability and possible applications, from food packaging film (Hansen and Plackett, 2008) to hydrogels (Lindblad et al., 2005) make them a desirable compound to extract. GGM have been succesfully recovered from process streams in thermomechanical pulp mills that use Norway spruce (*Picea abies*) as raw material (Persson et al., 2010).

GGM consist of a backbone of mannose and glucose with galactose side groups and can be partly acetylated (Hartman et al., 2006), the ratio galactose:glucose:mannose can vary but is commonly 1:1:3 (Timell, 1967). GGM from thermomechanical pulp mills have an average molecular weight of 10-20 kDa (Hartman et al., 2006; Thuvander and A. S. Jönsson, 2016). Other estimates for the molecular weight of GGM from softwood are in the range of 16-24 kDa (Lundqvist et al., 2002) and up to 45-64 kDa (Willför et al., 2003). The size estimates vary due to natural variations in the wood, extraction method and size estimation method.

2.1.3 Dextran

Dextrans are a polysaccharide and have a backbone with small side chains, all made of D-glucose (Caligur, 2008). They can vary largely in size but have a molecular weight of at least 1 kDa and their configuration depends on the bacteria strain used in the production. Dextrans have a wide variety of usages. Beside others they are used as a standard for size exclusion chromatography and the determination of the molar weight of GGM (Willför et al., 2003; Lundqvist et al., 2002; He et al., 2018). Dextrans are also a common model compound for polysaccharides in membrane filtration (Rudolph et al., 2019). Therefore dextran was selected as a model compound for GGM in this study.

2.1.4 Glucose

D-glucose is the most common monosaccharide in nature. It is a six-carbon sugar and has a cyclic form (Schenck, 2006). Since it is a comoponent in GGM it was selected as a model compound for GGM in this study.

2.2 Quartz crystal microbalance with dissipation monitoring

QCM-D is a method that can be used to study solvated interfaces between a solid surface and a fluid (Reviakine, Johannsmann, and Richter, 2011). QCM-D is based on monitoring how the piezoelectric properties of quartz crystals change with changes in the surrounding media (Liu and Zhang, 2013). A piezoelectric material produces an electric potential when compressed. The reverse effect is also possible: the material deforms when exposed to an electric field. The QCM-D crystal deforms in a thickness-shear mode, creating a transverse wave where the crystal oscillates transversely to the direction the wave propagates. When an alternating voltage is applied at a frequency close to the resonating frequency of the crystal, a standing wave is created. The resonating frequency depends on the thickness of the crystal, which makes a quartz crystal an excellent mass sensor, as long as any added layer is thinner than the quartz crystal itself. The Sauerbrey relationship, Equation 2.1, directly relates the adsorbed mass per unit area, Δm_f, to the change in oscillation frequency Δf. n is the overtone number and C is the mass sensitivity constant. For a quartz crystal with a fundamental frequency of 5 MHz, the mass sensitivity constant is 17.7 ng/(cm^2 Hz) (Qsense Biolin Scientific, 2020).

$$\Delta m_f = -\frac{C}{n}\Delta f_n \tag{2.1}$$

The dissipation, D in Equation 2.2, depends on the energy stored in the oscillating system, E_s, and the energy dissipated with each oscillation, E_d. This is measured by intermittently turning off the voltage applied and detect how fast the energy dissipates. Since the voltage can be turned on and off over 200 times per second, QCM-D can study how the adsorbed layer changes in real-time with good resolution (Biolin Scientific, Sweden, n.d.).

$$D = \frac{E_d}{2\pi E_s} \tag{2.2}$$

The Sauerbrey relation, Equation 2.1, applies when the added mass is rigidly adsorbed and when surrounded by air or vacuum (Liu and Zhang, 2013). It can be applicable for liquid systems if the dissipation shift is sufficiently small (Reviakine, Johannsmann, and Richter, 2011). For a 5 MHz crystal, sufficiently small is defined as in Equation 2.3.

$$\frac{D_n}{-\Delta f_n/n} << 4 \cdot 10^{-7} Hz \tag{2.3}$$

Depending on the properties of the adsorbed substances the adsorbed layer can either be considered laterally homogeneous or formed by discrete particles (Reviakine, Johannsmann, and Richter, 2011). In both cases, the QCM-D sensor might also register some of the solvent. In a laterally homogeneous layer, the layer is solvated and Δm_f the sum of the mass of the adsorbent and some mass of the solvent. For a layer of discrete particles, a close volume of entrapped solvent around each particle is detected. For a higher degree of coverage, the volumes start to overlap and the amount of entrapped solvent per adsorbed particle decreases. This increases the sensitivity of QCM-D sensor at low surface coverage and decreases the sensitivity at high surface coverage. In both cases a combination of QCM-D with mass-sensitive optical techniques, such as surface plasmon resonance or ellipsometry, can differentiate between the mass of the adsorbate and the mass of the solvent.

The Q-sense Dfind v1.2.1 software has two layer models based on the Sauerbrey relation. The model 'Sauerbrey' calculates the adsorb mass based on a selected overtone. The 'Composite Sauerbrey' calculates the adsorbed mass through the Sauerbrey relation for all given overtones and presents the average solution (Qsense Biolin Scientific, Sweden, n.d.).

In cases where the Sauerbrey relation is not applicable, the Voigt model can be used to describe the viscoelastic layer (Liu and Zhang, 2013). This is based on the assumption that the adsorbed layer is homogeneous and with a uniform thickness and it is surrounded by a semi-infinite Newtonian fluid with no-slip condition at the interface. However, the Voigt model has received some critique recently and there are other models to describe the viscoelastic layer (Reviakine, Johannsmann, and Richter, 2011). The Q-sense D-find software has two layer models based on the Voigt model. The 'Dfind Broadfit' evaluates the data and chooses the best fit for each timestep. The 'Dfind Smartfit' assumes that the data represents smooth

changes in the surface layer and presents, if found, the two best solutions that give a continuous result (Qsense Biolin Scientific, Sweden, n.d.).

2.3 Adsorption

One mechanism for membrane fouling is adsorption (Dal-Cin et al., 1996). Adsorption on the membrane surface and onto the walls of the membrane pores causes reduced flux and efficiency of the membrane.

Adsorption is when a substance attaches to a surface and desorption is when the substance detaches (Atkins and De Paula, 2010).

$$A \underset{r_{des}}{\overset{r_{ads}}{\rightleftharpoons}} A_s \tag{2.4}$$

The adsorption can be divided into physisorption and chemisorption. Physisorption is when the van der Waals interaction binds the adsorbate and the adsorbent and chemisorption is when the adsorbate binds with covalent bonds to the adsorbent. The behaviour of the adsorption process can further be described by an adsorption isotherm which describes the amount adsorbed at equilibrium at a constant temperature but varying pressure (for solid-gas adsorption) or concentration (solid-liquid adsorption). There are several isotherms such as the Langmuir, Freundlich, BET or Temkin, but most of them are empirical. Another important aspect is the adsorption kinetics or the rate at which the adsorbate adsorbs to the surface (Qiu et al., 2009). Some kinetic models describe only the adsorption/desorption process, such as pseudo order models, while others also include the diffusion of the adsorbate to the adsorption site, such as liquid film diffusion models.

Cherkasov (2020) outlined the difficulties with adsorption studies of solid-liquid adsorption and the importance of not using results for solid-gas adsorption to describe a solid-liquid system. Experimentally, the adsorption can be estimated either by measuring the substance from the bulk or by measuring the substance adsorbed from the surface. Measurements in the bulk may overestimate the adsorption if any unforeseen chemical reaction consumes the substance. It is also prone to large errors if the relative decrease in bulk concentration is too small (< 5 %). Measurements on the surface can be done by spectroscopy or gravimetry. Gravimetry, like QCM,

is a common method to study gas systems (Atkins and De Paula, 2010), but are less reliable in liquid systems due to the presence of a solvent (Cherkasov, 2020). Desorption experiments have the same problems of unforeseen reactions, but in this case, they underestimate the adsorption.

When analysing the data and fitting isotherm parameters, thermodynamic parameters and kinetic parameters several things should be considered (Cherkasov, 2020):

1. The model assumption should be fulfilled and extrapolation of results should be avoided as small errors in the model or parameters might lead to large errors.
2. Parameters should be determined without using linearised models as it can introduce additional errors when extrapolated.
3. Curve fitting should be done with an objective function of weighed residual rather than absolute errors. Using absolute error, which is the most common in software like Excel, will fit better to high concentrations than to low concentrations due to the fact that lower concentrations have lower absolute errors and therefore neglected compared to the larger absolute errors of the higher concentrations. Using weighed residuals mitigates this problem.
4. The confidence interval for the parameters should be determined using the Monte-Carlo method.
5. To determine the adsorption kinetics, it is also important to not include too many data points once the process has reached equilibrium as it might skew the fit of the parameters and cause unnecessary errors.

2.3.1 Langmuir adsorption

The basic assumptions for the Langmuir model are(Atkins and De Paula, 2010):

1. The adsorbing components will only form one layer, a so-called monolayer.
2. Adsorption sites are equivalent and the adsorption surface is uniform.
3. There is no interaction between adsorbed molecules and adsorbed molecules do not affect the ability for other molecules to adsorb.

When the adsorption/desorption reaction follows the Langmuir kinetics the adsorption reaction can be expressed as in Equation 2.5 and the rate depends on the adsorption coefficient k_{ads}, the bulk concentration c_A, and the available adsorption sites $\Gamma_s - c_s$, where Γ_s is the maximum possible concentration of adsorption sites and c_s, the current concentration of the adsorbed substance (Nilsson and Andersson, 2018). The rate of desorption can be expressed as in Equation 2.6 and depends on the desorption coefficient k_{des} and the concentration of the current adsorbed substance.

$$r_{ads} = k_{ads} \left(\Gamma_s - c_s\right) c \tag{2.5}$$

$$r_{des} = k_{des}\, c_s \tag{2.6}$$

The difference between the adsorption rate and the desorption rate forms the overall sorption rate as stated in Equation 2.7.

$$r = k_{ads} \left(\Gamma_s - c_s\right) c - k_{des}\, c_s \tag{2.7}$$

When the adsorption/desorption reaction is at equilibrium (r=0) the concentration of the adsorbed substance can be calculated using the Langmuir isotherm, Equation 2.8, where K is the ratio of k_{ads} to k_{des}.

$$c_s = \frac{K\,\Gamma_s\, c}{1 + Kc} \tag{2.8}$$

Reference study

A method to measure the Langmuir adsorption kinetics with QCM-D has been presented by Wu et al. (2007). They determined the adsorption kinetics of the polymer poly(*N*isopropylacrylamide) (PNIPAM) onto a gold surface using QCM-D. They assumed that the surface coverage θ of PNIPAM can be described as in Equation 2.9 which is equivalent to the Langmuir kinetics in Equation 2.7.

$$\frac{d\theta}{dt} = k_a \left(1 - \theta\right) c - k_d \theta \tag{2.9}$$

Integrating Equation 2.9 gives Equation 2.10 where the decay constant k_0 is described in Equation 2.11 and the equilibrium surface coverage θ_{eq} is described in Equation 2.12.

$$\theta = \theta_{eq} + (\theta_i - \theta_{eq})exp(-k_0 t) \tag{2.10}$$

$$k_0 = k_{ads}c + k_{des} \tag{2.11}$$

$$\theta_{eq} = \frac{c}{c + k_{des}/k_{ads}} \tag{2.12}$$

It was assumed that the Saurebrey relation applies (see Section 2.2). That gives that the difference in frequency shift Δf is proportional to the difference in surface coverage, $\Delta\theta$ and, in turn, proportional to $\exp(-k_0 t)$, Equation 2.13.

$$f(t) - f_{eq} \sim \Delta\theta = \theta - \theta_{eq}\ exp(-k_0 t) \tag{2.13}$$

To estimate the adsorption kinetics, Wu et al. filled the QCM-D chamber with a solution with a low concentration of PNIPAM and let it adsorb while measuring the frequency shift and dissipation change over time until the adsorption process reached equilibrium. Subsequently, they dosed a PNIPAM solution of higher concentration into the cell. The concentrations used were 2.5, 5, 10, 20, 40 and 80 ppm by weight. The experiments were performed at 20 °C.

The k_{ads} and k_{des} were found by first plotting $f(t) - f_{eq}$ for each concentration in a semilog-plot against time. Secondly, an apparent straight line was fitted to the data for each concentration using a least square-root fit where the slopes were the decay constant, k_0. The decay constant was then plotted as a function of PNIPAM concentration and k_{ads} and k_{des} was found by a linear fit according to Equation 2.11. The parameters were determined as k_{ads}=152.2 $1/(\mathrm{M} \cdot \mathrm{s})$ or $775.1 \times 10^{-4}\ 1/(\mathrm{wt\%} \cdot \mathrm{s})$ and k_{des}=$1.746 \times 10^{-4}\ 1/\mathrm{s}$

For the purpose of my study the frequency shift at equilibrium, Δf_{eq}, was defined as the average frequency shift for the last 5 minutes of the measurement period, assuming that the system reached equilibrium at that time.

2.3.2 Pseudo-first- and second-order models

Pseudo-models are models based on the concentration of the adsorbent on the adsorbate instead of the remaining concentration in the solution (Moussout et al., 2018). Table 2.1 presents the kinetic model and both the linear and non-linear form of the integrated model.

Table 2.1 – Kinetic model for pseudo-first- and pseudo-second-order models in non-linear and linear form

Order	Kinetic model	Non-linear form	Linear form
1	$\frac{dq_t}{dt} = k_1(q_e - q_t)$	$q_t = q_e(1 - e^{-k_1 t})$	$ln(q_e - q_t) = ln(q_e) - k_1 t$
2	$\frac{dq_t}{dt} = k_2(q_e - q_t)^2$	$q_t = \frac{q_e^2 k_2 t}{q_e k_2 t + 1}$	$\frac{t}{q_t} = \frac{1}{k_2 q_e^2} + \frac{1}{q_e} t$

The pseudo-first-order has been used to study the adsorption of oxalic acid and malonic acid onto charcoal (Qiu et al., 2009). More recently it has been used to study the adsorption of dyes from wastewater or aqueous solutions onto solids such as palm trunk fibre. The pseudo-first-order model was valid at the initial stages of adsorption (Moussout et al., 2018).

The pseudo-second-order model has been used to describe the adsorption of metal ions, dyes, oils and organic substances from aqueous solutions but also adsorption of organic pollutants onto non-polar polymeric adsorbents (Qiu et al., 2009). The pseudo-second-order model is best suited for chemisorption and not suitable for physical adsorption such as organic pollutants onto non-polar polymers. The pseudo-second-order model tends to be more applicable than the pseudo-first-order, however this may be due to mathematical reasons rather than real physical ones (Moussout et al., 2018). The use of non-linear and linear versions of the pseudo-order models have been shown to affect which pseudo-model has the best fit, even when fitted to the same set of data.

3 Materials and Methods

3.1 Materials

The polysulfone polymer used was the same as in the production of commercial UF membranes UFX5-pHt and UFX10-pHt by Alfa Laval, Denmark. The PSU polymer solution was dissolved in 99 % dichloromethane (DCM) solution (Merck, Germany). The final concentration of PSU was 0.3 wt%.

D-Glucose (Merck KGaA, Germany) was diluted with deionized water to 0.02, 0.05, 0.08, 0.11 and 0.15 g/L. Dextran 15 (SERVA, Germany) with a molecular weight in the range of 15 000 g/mol to 20 000 g/mol was diluted with deionized water to 0.0034, 0.0085, 0.017, 0.034, 0.068, 0.17, 0.34, 1.02 and 1.7 g/L. A molar weight of 17 000 g/mol was assumed for calculations.

The GGM used had been extracted from process water from a thermomecanical pulp mill. The process water had been sieved (45 µm Endecotts, UK) to remove fibers and particles and stored frozen until use. Microfiltration of process water had been performed with a tubular, silica carbide ceramic membrane from LiqTech International A/S, Denmark, with a cut-off of 0.04 µm. The membrane had 19 parallel feed flow channels, each with a diameter of 4.8 mm. Microfiltration had been run at a TMP of 0.6 bar, at 80 °C (to have similar conditions as in the mill) and a crossflow velocity of 2 m/s until a volume reduction (VR) of 98 % had been reached. To reduce the salt content, the permeate from MF had then been diafiltrated through a batch ultrafiltration with deionized water as dilutant. A UFX5-pHt membrane had been used at a TMP of 2 bar, 70 °C and a cross flow velocity of 0.41 m/s. The diafiltration factor DF $= V_b/V_s$ calculated from the volume of the dilutant V_b and the volume of the solution V_s had been set to DF = 2. To further increase the purity, anti-solvent precipitation had been conducted according to Zasadowski et al. (2014) with 70 % acetone for a duration of 3 h. The precipitated GGM was assumed to have a molar weight of 10 000 g/mol. The GGM was diluted in deionized water to solutions with concentrations of 0.0001, 0.001, 0.005, 0.01, 0.05 and 0.1 g/L.

3.2 QCM-D measurements

The QCM-D experiments were performed with a Q-Sense E4 system (Biolin Scientific, Sweden) with QFM 401 flow modules connected to a peristaltic pump. The sensors used were Qsensor QSX 301 Gold (Biolin Scientific/Q-Sense, Sweden). They had a gold surface, a fundamental resonant frequency of 4.95 MHz, a thickness of 0.3 mm and a diameter of 14 mm. Figure 3.1 show the QCM-D equipment used.

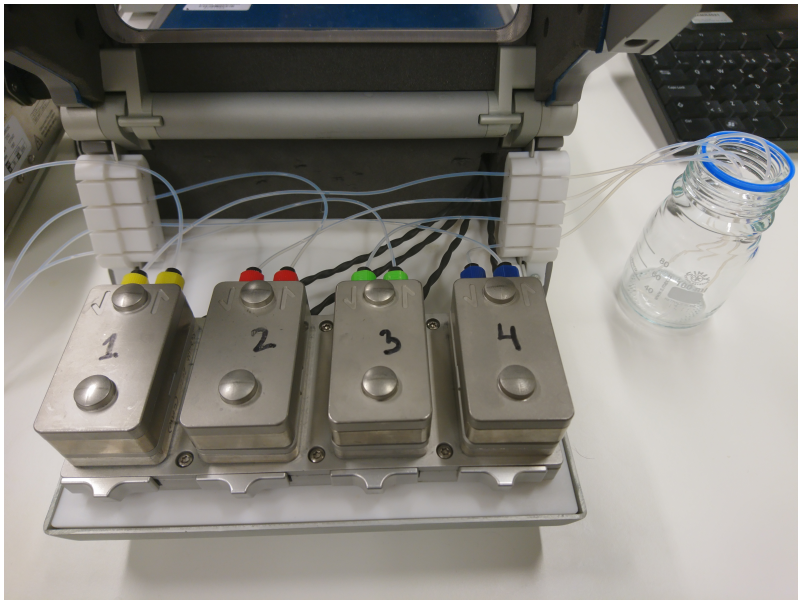

(a) The setup with the four QCM-D modules run in parallel with the sample vial to the right and the peristaltic pump to the left (outside of image).

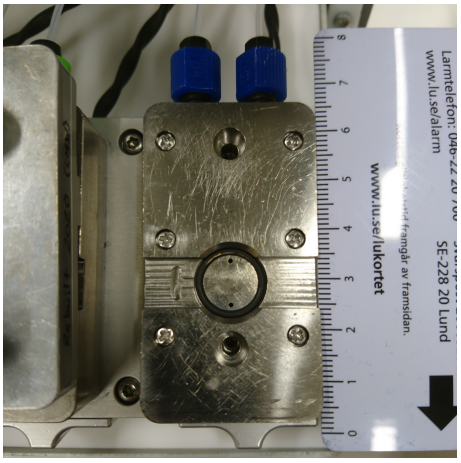

(b) Inside of QCM-D module showing the sensor chamber ceiling limited by the rubber ring.

(c) Quartz crystal sensor with gold surface.

Figure 3.1 – QCM-D equipment and set-up.

3.2.1 Pre-cleaning

The uncoated sensors were cleaned by rinsing with Milli-Q water followed by 98 % ethanol and air-dried with nitrogen gas. Then they were exposed to UV light and ozone for 10 minutes at 2×10^{-1} bar in a plasma cleaner PDC-3XG (Harric Scientific Co., USA).

The pre-cleaning was done before spin-coating and before the experimental measurement on uncoated sensors.

3.2.2 Spin-coating

Before spin-coating, the frequency and dissipation of the sensors were measured in degassed Milli-Q water at 25 °C at a flow rate of 0.200 mL/min during 5-10 minutes.

The sensor was spin-coated by dropping a solution with 0.3 wt% PSU in DCM onto the sensor and spinning it for 30 s at 4 000 rpm and 2000 s^{-2}. This was done in a LabSPin6/8 (Süss+MicroTec, German). The spin-coated sensor was left to dry for 24 h.

3.2.3 QCM-D experiments

The same eperimental procedure was used for both PSU-coated sensors and uncoated sensors. The adsorption measurements were performed at 25 °C. All solutions were degassed for 5 minutes in an ultrasonic bath before measurement. The baseline for frequency and dissipation was measured in Milli-Q water at 25 °C at a flow rate of 0.200 mL/min during 5-10 minutes. Then the lowest concentration was pumped into the cell at 0.200 mL/min. The pump was stopped when a change in signal from all sensors could be observed or after 2 min, whichever came first, and the solution was left in the cell until the signal seemed to have reached equilibrium. This could take from a few minutes to up to 1.5 hours. The cell was then flushed with Milli-Q water until the frequency went back to the baseline, reached a new equilibrium or had returned to values similar to before the start of the flushing, depending on the time available. Then a higher concentration was pumped into the cell. Four replicates were run in parallel for each experiment, but usually only yielding duplicates or triplicates of the result due to baseline drift in individual sensors or air bubbles in the system.

3.2.4 Cleaning PSU-coated sensors

After use, the PSU-coated sensors were cleaned by being ultrasonicated in a DCM solution for 15 minutes and stored in the DCM solution for at least 24 h. Then they were ultrasonicated again for 15 minutes, rinsed with deionised water and ethanol, air-dried and cleaned in an alkaline piranha solution (NH_4OH(25 %):H_2O_2(20 %):water= 1:1.5:5 v/v/v conc.) for 15 minutes at 75 °C. Finally, they were rinsed again with deionised water and air-dried for storage.

3.2.5 Data processing

The data was processed in EXCEL 2016 (Microsoft, USA) and for curve-fitting the solver method GRG nonlinear was used. Evaluations based only on frequency shift was done for the 3rd overtone. Layer modelling was done in Q-Sense Dfind 1.2.1.

3.3 COMSOL Model

COMSOL multiphysics® v.5.3 was used to perform simulations. Two models were developed for this project, one reference model with adsorption kinetics based on results from Wu et al. (2007), and one model for GGM with experimentally determined adsorption kinetics.

3.3.1 QCM-D geometry model

The interior of a QCM-D flow module consists of an inlet flow channel, the sensor chamber and an outlet flow channel (Biolin Scientific, Sweden, 2019). The inlet flow channel is constructed in a serpentine pattern to allow the fluid to stabilise at a set temperature. The sensor chamber contains the sensor fixed in place by supporting rubber rings. The inlet and outlet to the sensor chamber are placed in the bevelled ceiling (Biolin Scientific, Sweden, 2020). The QFM 401 flow module has a flow channel for approximately 100 µL (Biolin Scientific, Sweden, 2019). The sensor chamber contains approximately 40 µL, the inner diameter of the O-ring is 11.1 mm and the maximum distance between the sensor and ceiling is 0.6 mm at the centre of the cell (Biolin Scientific, Sweden, 2020). The inlet and outlet to the sensor chamber are 1.0 mm in diameter. The sensor chamber has a Reynolds number of approximately 0.2 at a flow of 0.1 mL/ min and 2.0 at 0.8 mL/ min. The tubing has a

diameter of 0.75 mm and is measured to be 32 cm to 33 cm long, making the volume of each tube 0.141 mL to 0.146 mL.

The inner volume of the sensor chamber was estimated to consist of a cylinder with a spherical cap forming the ceiling to comply with the maximum height, the diameter and the volume of the cell. The optimal height for the cylinder was 0.23 mm and 0.37 mm for the spherical cap. The space between the inlet and outlet is assumed to be 7.1 mm and the remaining distance to the rubber ring is assumed to be 1 mm for each opening. The flow cell is shown in figure 3.2.

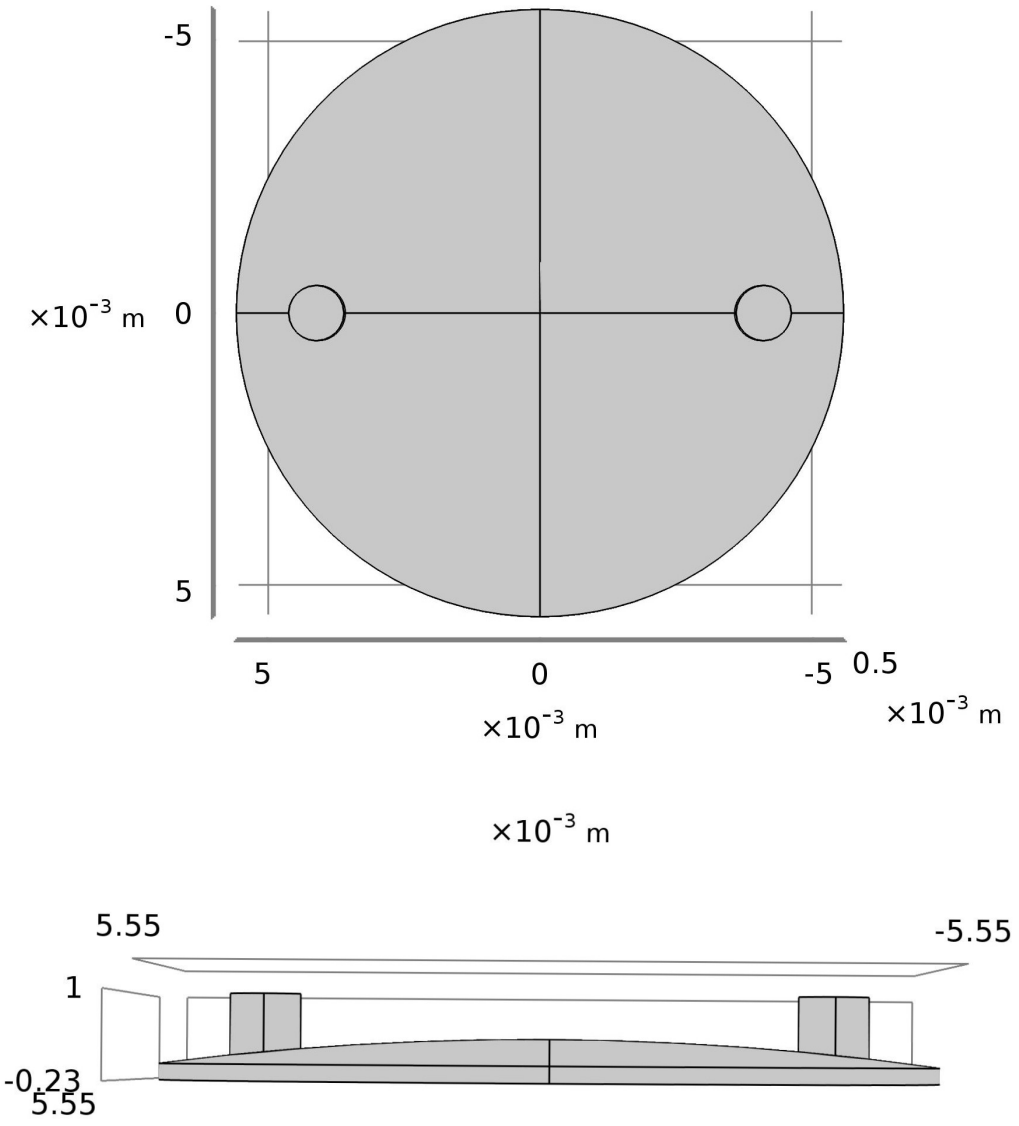

Figure 3.2 – Top view (top) and side view (bottom) of the QCM-D sensor chamber geometry.

3.3.2 Model Equations

The model equations are based on Comsol (n.d.) The system is modelled using three coupled physics in COMSOL. A General Form Boundary Partial Differential Equation (G. F. B. PDE) describes the adsorption surface, the Transport of Diluted Species physics describes the substance in the bulk and the Laminar Flow physics describes the fluid flow in the bulk.

The material balance for the surface consists of the accumulation $\frac{\delta c_s}{\delta t}$, the surface diffusion $\nabla \cdot (-D_s \nabla c_s)$, and the adsorption and desorption rate r.

$$\frac{\delta c_s}{\delta t} + \nabla \cdot (-D_s \nabla c_s) = r \tag{3.1}$$

The boundary condition for the surface is insulating according to Equation 3.2.

$$\mathbf{u} \cdot (-D_s \nabla c_s) = 0 \tag{3.2}$$

In the Transport of Diluted Species physics, the material balance in the bulk is described through a convection-diffusion equation, Equation 3.3, where D_A is the diffusion coefficient for the substance and the $\mathbf{u}$ is the vector field describing the velocity for the flow and c_A is the bulk concentration of the substance.

$$\frac{\delta c_A}{\delta t} + \nabla \cdot (-D_A \nabla c_A + c_A \mathbf{u}) = 0 \tag{3.3}$$

The material balance in the bulk is coupled with the surface through the boundary condition in Equation 3.4, where the right-hand side is the negative of the overall rate of adsorption.

$$\mathbf{n} \cdot (-D_A \nabla c + c\mathbf{u}) = -k_{ads}\, c\, (\Gamma_s - c_s) + k_{des}\, c_s \tag{3.4}$$

All initial conditions, boundary conditions and mass balances are summarised in Table 3.1.

Table 3.1 – Mass balances, boundary conditions and initial conditions

Physics	**Conditions**	
G. F. B. PDE	**Mass balance**	$\frac{\delta c_s}{\delta t} + \nabla \cdot (-D_s \nabla c_s) = r$
	Boundary	$\mathbf{u} \cdot (-D_s \nabla c_s) = 0$
	Initial values	$c_s = 0$
Transport of Diluted Species	**Mass balance**	$\frac{\delta c_A}{\delta t} + \nabla \cdot (-D_A \nabla c_A + c_A \mathbf{u}) = 0$
	Boundaries	
	Sensor surface	$\mathbf{n} \cdot (-D_A \nabla c_A + c_A \mathbf{u}) = -r$
	Conc. inflow	$c_i = c_{0.cA}$
	Outflow	$-\mathbf{n} \cdot D_i \nabla c_i = 0$
	No flux	$-\mathbf{n} \cdot \mathbf{N}_i = 0$
	Initial value	$c_A = 0$
Laminar Flow	**Mass balance**	$\rho \frac{\partial \mathbf{u}}{\partial} + \rho(\mathbf{u} \cdot \nabla)\mathbf{u} = \nabla \cdot [-\rho \mathbf{l} + \mu(\nabla \mathbf{u} + (\nabla)^T] + \mathbf{F}$
		$\rho \nabla \cdot (\mathbf{u}) = 0$
	Boundaries	
	Laminar inflow	$L_{entr} \nabla_t \cdot [-p\mathbf{l} + \mu(\nabla_t \mathbf{u} + (\nabla_t \mathbf{u})^T)] = -p_{entr}\mathbf{n}$
	Outlet pressure	$[-p\mathbf{l} + \mu(\nabla \mathbf{u} + (\nabla \mathbf{u})^T)]\mathbf{n} = -\widehat{p}_0 \mathbf{n}$
		$\widehat{p}_0 <= p_0 = 0$
	Initial values	$\mathbf{u} = [0, 0, 0]$
		$p = 0$

3.3.3 Diffusivity

The model of the diffusion of the reference system with PNIPAM was based on the characterisation done by Yohannes et al. (2005). They used asymmetrical flow field-flow fractionation and a polyethylene oxide (PEO) standard to determine the molar weight of PNIPAM. The relationship between the diffusion and the molar weight distribution according to the PEO standard is shown in Equation 3.5 where D_A is the diffusivity in cm^2/s and M is the molar mass in mol/g. This was integrated into COMSOL as a global parameter.

$$log(D_A) = -0.48913 \cdot log(M) - 4.29114 \tag{3.5}$$

The diffusivity for GGM was estimated through Wilke-Chang's equation, Equation 3.6 (Alveteg, 2020). Where the ϕ is the dimensionless association parameter for water, in this case 2.6, T is the temperature in Kelvin, $\mu_{solution}$ is the viscosity for water, $M : solvent$ is the molar weight of water and $\tilde{V}_{A_b}$ is the molar volume of the solute (GGM). All units are in SI-units.

$$D_{AB} = 5.878 \cdot 10^{-17} \frac{T\sqrt{\phi M_{solvent}}}{\mu_{solution}(\tilde{V}_{A_b})^{0.6}} \tag{3.6}$$

The molar volume of GGM $\tilde{V}_{A_b}$ is estimated from their molecular weight. GMM has a molecular weight of 16 000-24 000 g/mol which corresponds to a degree of polymerisation (DP) of 100-150 (Lundqvist et al., 2002). Assuming that there is a linear relationship between DP and molar weight, it can be expressed as in Equation 3.7

$$DP = 0.00625 \cdot M_w \tag{3.7}$$

From the DP the molar volume is calculated from Equation 3.8, where $V_i = 1.11 \times 10^2\,cm^3/mol$ is the molar volume of monosaccharides. Equation 3.8 is a simplified version of Equation 3.9 by Pérez Nebreda et al. (2019) used to describe the hydrolysis of GGM. Here DP is fixed to 100 and the total sugar conversion, X_{TOT}, varies from 0 (no hydrolysis) to 1 (total hydrolysis). However, the simplified version should be sufficient since the difference between the two models is less than 5 % for DP >16 for Equation 3.8 and X_{TOT} >0.84 for Equation 3.9.

$$\tilde{V}_{A_b} = DP \cdot V_i \tag{3.8}$$

$$\tilde{V}_{A_b} = (X_{TOT} + DP_{100} \cdot (1 - X_{TOT})) \cdot V_i \tag{3.9}$$

Equation 3.7 and 3.8 were integrated with COMSOL as parameters, while Equation 3.6 was integrated as a variable because the viscosity of water was described by the material properties model for water provided by COMSOL.

Surface diffusivity, D_s, was assumed to be $0\,\mathrm{m}^2/\mathrm{s}$ for both PNIPAM and GGM. This means that the adsorbed substance is fixed in place on the surface and can only move from its position by desorbtion.

4 Results

4.1 Experimental results

This section presents the adsorption measurments done with QCM-D. Starting with Glucose on PSU, then dextran on gold and PSU, followed by GGM on gold with estimation of adsorption parameters for all 3 adsorption kinetics and finally GGM on PSU with estimation of adsorption parameters for Langmuir kinetics.

4.1.1 Glucose

In the experiment with glucose onto PSU, no significant adsorption kinetics could be observed. See Appendix 1 for details.

4.1.2 Dextran

Figure 4.1 shows the frequency shift and dissipation for dextran on gold from 0.17 g/L to 1.7 g/L for dextran with a molar weight of 17 kDa. Due to time constraints, the experiments were performed without flushing with water between each concentration. Apart from 0.17 g/L for sensor 1 the frequency shift is quite small, 1 Hz or less, for each concentration. The adsorption seemed to reach saturation before the pump was stopped since the frequency shift stayed constant once the pump was stopped.

Figure 4.2 shows the frequency and dissipation shift for dextran on PSU from 0.0034 g/L to 0.068 g/L for dextran with a molar weight of 17 kDa. Sensor 1 and 2 show some initial baseline drift since the frequency shift becomes positive. For all sensors the frequency shift at the different concentrations are very similar and very small.

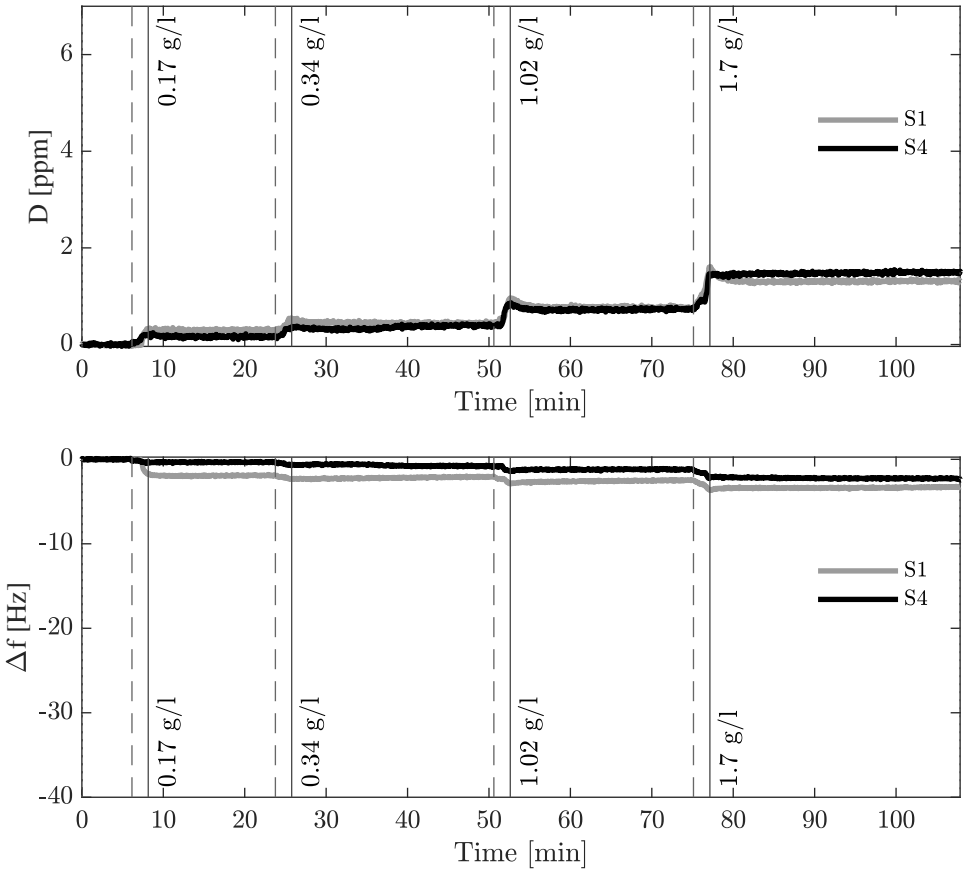

Figure 4.1 – Dissipation (upper) and frequency shift (lower) for dextran on gold. Dashed lines show when a new concentration is pumped into the cell and solid lines show when the pump is turned off for each concentration.

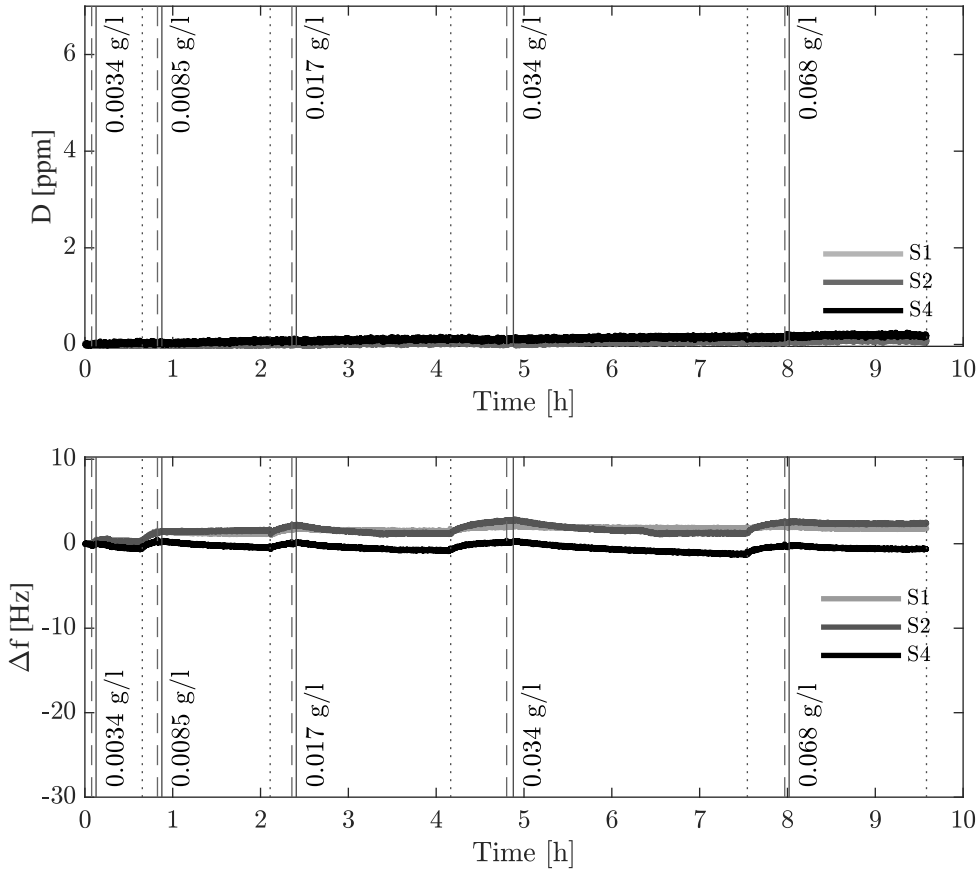

Figure 4.2 – Dissipation (upper) and frequency shift (lower) for dextran on PSU. Dashed lines show when a new concentration is pumped into the cell, dotted lines show when the cell is flushed with water and solid lines show when the pump is turned off for each concentration.

4.1.3 GGM on Gold

The frequency and dissipation shifts for GGM on gold are shown in figure 4.3. There is notable interaction, since the change in Δf increases with increasing concentration. The spikes at the beginning of pumping with Milli-Q water are probably caused by the remaining GGM solution in the tube flowing over the sensor before the water reached the sensor chamber.

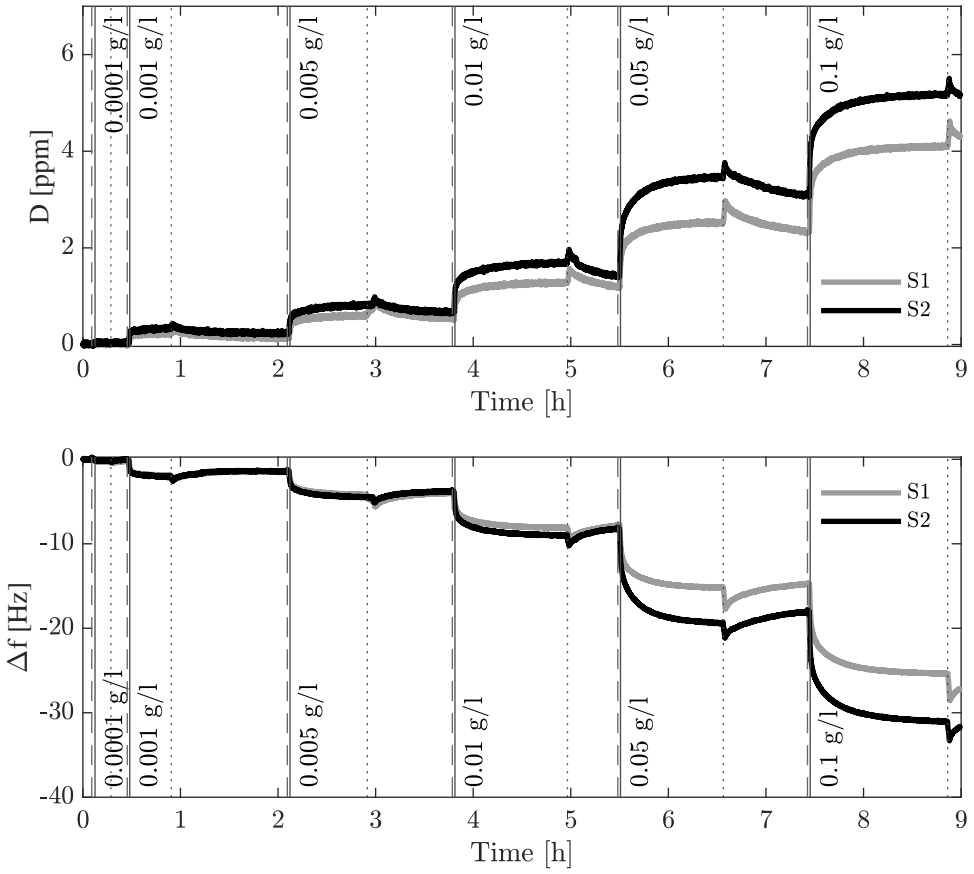

Figure 4.3 – Shows dissipation (upper) and frequency shift (lower) at third overtone for GGM using a gold-coated sensor. Dashed lines mark pumping of new concentration, solid line marks beginning of adsorption period, dotted line marks the end of the adsorption period followed by flushing with water.

To estimate the adsorption parameters, the experiment was evaluated according to the method used for in the reference system (Section 2.3.1). Figure 4.4 is a semi-logarithmic plot, showing the difference between the frequency shift, Δf, and the frequency shift at equilibrium, Δf_{eq}, for each concentration depending on time. The solid lines are functions on the form $y = 10^{kx+m}$ and were fitted to the data through least square fit for each concentration. The dotted line for 0.0001 g/L for Sensor 2

was fitted the same way. However, it extends to be 10^{-30} and the graph had to be cropped to increase clarity.

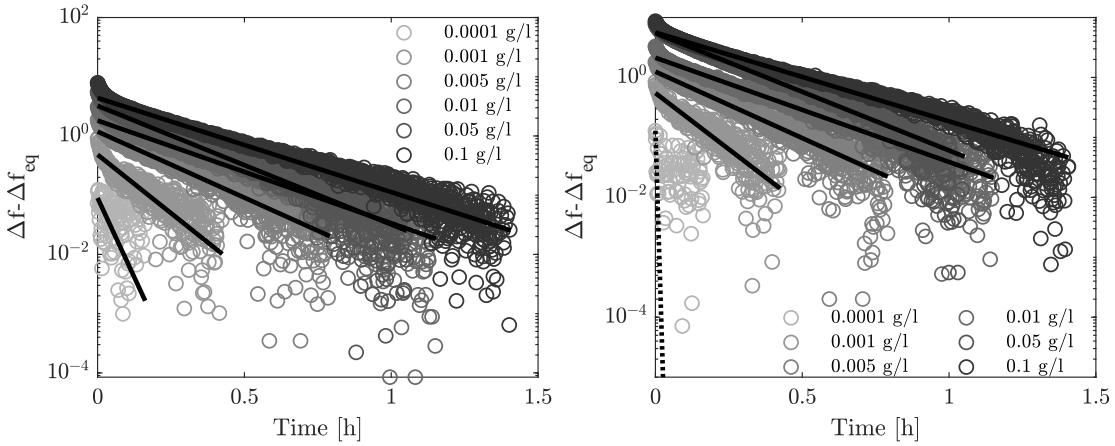

Figure 4.4 – Difference in frequency shift between time and equilibrium for Sensor 1 (S1, left) and Sensor 2 (S2, right) on a semi-log plot. The time is given from the beginning of each concentration. Solid lines are least-square root fit for each concentration. The dotted line (0.0001 g/L, S2) extends outside the plot window to $\Delta f - \Delta f_{eq} = 10^{-30}$. Note: Negative values are not shown.

The slopes of the fitted lines in Figure 4.4 are the negative of the decay constant, k_0 in Equation 2.10 and Equation 2.12 in Section 2.3.1. Figure 4.5 shows the decay constant plotted against the initial bulk concentration. The expected outcome was a linear dependence on the concentration according to Equation 2.12, this is not the case for the GGM, Figure 4.5 rather shows an exponentially decreasing rate constant that seems to reach a limit around $0.0005\,s^{-1}$ for the concentrations higher than 0.01 g/L.

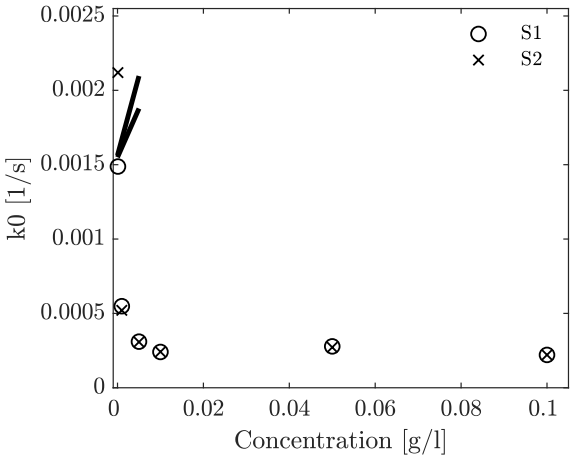

Figure 4.5 – Decay constants, k_0, for GGM on gold at different initial bulk concentrations. NB: The break in the y-axis

To evaluate the data with pseudo-order models it is necessary to know the surface concentration of adsorbent on the sensor surface. Figure 4.6 shows the result of 4 layer models provided by Dfind for 0.1 g/L for Sensor 1. Smartfit yields two results, Smartfit 1 and Smartfit 2, Broadfit gave a result that is either close to Smart fit 1 or, in this case, Smartfit 2. Sauerbrey R is the result of the Sauerbrey equation for overtone 3 and Sauerbrey C is the Composite Sauerbrey function based on overtone 3, 5, 7 and 9. The condition to apply Sauerbrey, given in Equation 2.3, averaged on 9.01×10^{-7} Hz, for Sensor 1, and 9.75×10^{-7} Hz, for Sensor 2, for overtone 3, 5, 7 and 9 during all measurement periods. This is larger than 4×10^{-7} Hz which is the limit to evaluate the adsorbed mass with Sauerbrey only. Smartfit 2 was chosen to evaluate the surface concentration of adsorbed GGM based on the frequency shift and dissipation, except for the bulk concentration 0.0001 g/L where Broadfit was used since the Smartfit did not find a solution for that concentration.

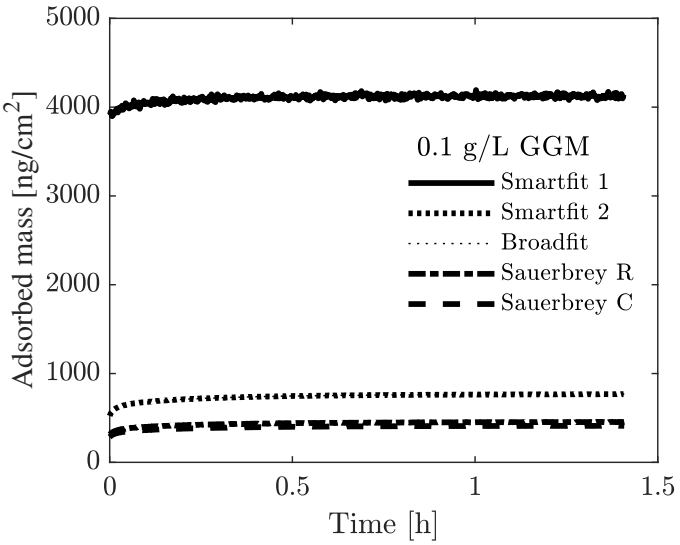

Figure 4.6 – The result of different layer models provided by D-find for 0.1 g/L in sensor 1. Smarfit 1 and 2 are provided by the Smartfit model, Broadfit is almost identical to Smartfit 2. Sauerbrey R is based on the third overtone and Sauerbrey C is based on overtone 3, 5, 7 and 9.

A linearised pseudo-first-order model was fitted to the data as described in Section 2.3.2. The results are shown in Figure 4.7. The grey lines are the least square fit of the linearised pseudo-first-order model to the data. The fit is very poor, the coefficients of determination R^2 are in the range of -5 to -46.

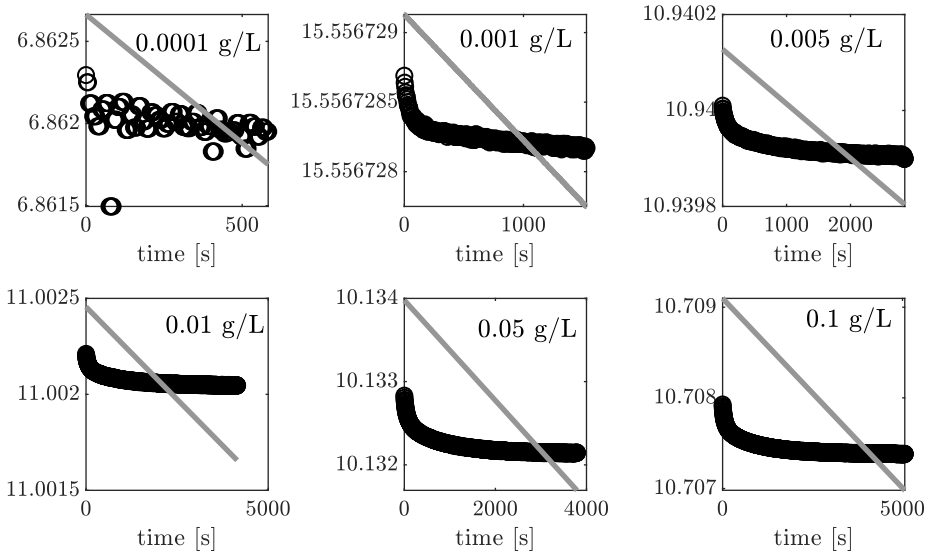

Figure 4.7 – $\ln(q_e\text{-}q_t)$ against time. Black circles are the data from sensor 1 and the grey line is the least square fit.

The data for GGM on gold was also used to fit a linearised pseudo-second-order model. In Figure 4.8 time divided by the surface concentration is plotted against the time for each concentration and the solid lines are the least-square fit of the model to each concentration. The coefficient of determination was 0.74 for 0.0001 g/L for Sensor 2, but for the other concentrations it was above 0.97, which indicates a good fit of the model to the data.

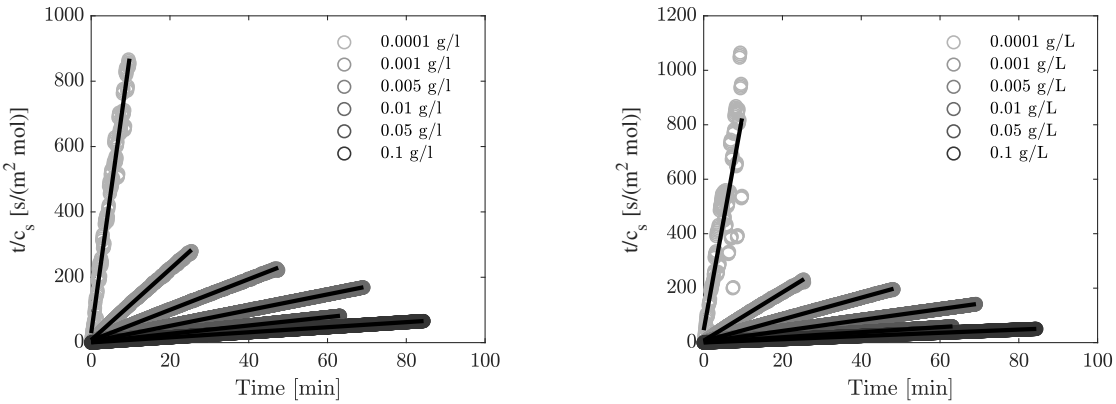

Figure 4.8 – Non-linear pseudo-second-order model for GGM on gold for Sensor 1 (left) and Sensor 2 (right). Time divided by surface concentration is plotted against time since the starting time for the concentration. Solid lines are least square fit of the model to data

Figure 4.9 shows the q_e-values and the k-values were plotted against their initial bulk concentration, here called x. The q_e was fitted with the expression $q_e = a \cdot e^{bx} + c$ with a=−112, b=−133 and c=118. The model had a coefficient of determination of 0.94. The coefficient k_2 was fitted with the equation $k_2 = a \cdot x^b$, where a=6.79×10^{-6} and b=−0.781. The expression had a coefficient of determination of 0.90. The expression for q_e and k_2 are both in SI-units with the concentration given as mol/m^3.

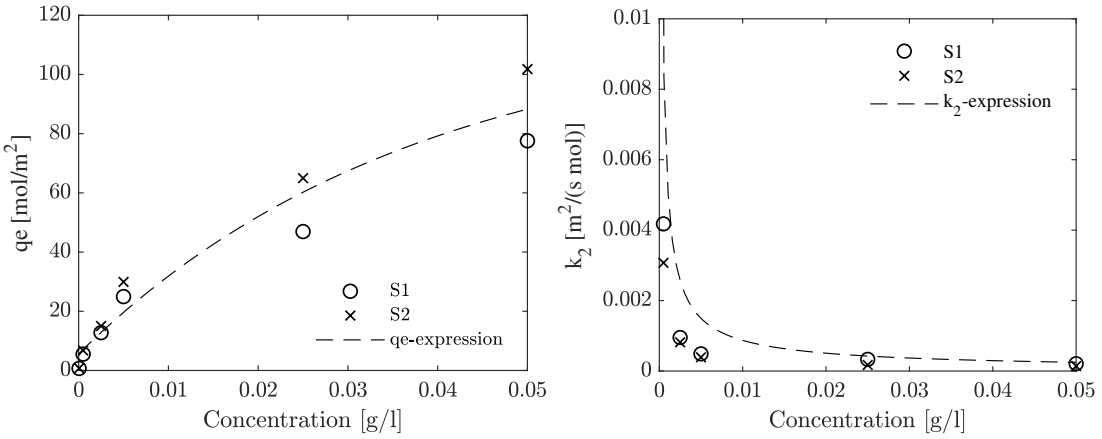

Figure 4.9 – Parameters q_e (left) and k_2 (right) against initial bulk concentration. Dashed line are least-square fit of the model to data. Note: k-values for both sensors at 0.0001 g/L are 0.0710 and 0.0389 respectively and outside of the plotted range.

4.1.4 GGM on PSU

Figure 4.10 shows the frequency and dissipation shift for the third overtone for GGM on PSU for one experimental run (for the other experimental run see B). GGM on on PSU shows weaker adsorption kinetics compared to GGM on gold.

Same as for the results of GGM on gold, Section 4.1.3, the results for GGM on PSU were plotted on a semi-logarithmic scale with the difference between the frequency shift δf and the frequency shift at equilibrium against time, as shown in figure 4.11. The solid lines are the least square-root fit of the data. When performing the least square-root fit to the data, the solver could not find a converging solution for several of the concentrations, and the solid lines are therefore not shown for these concentrations.

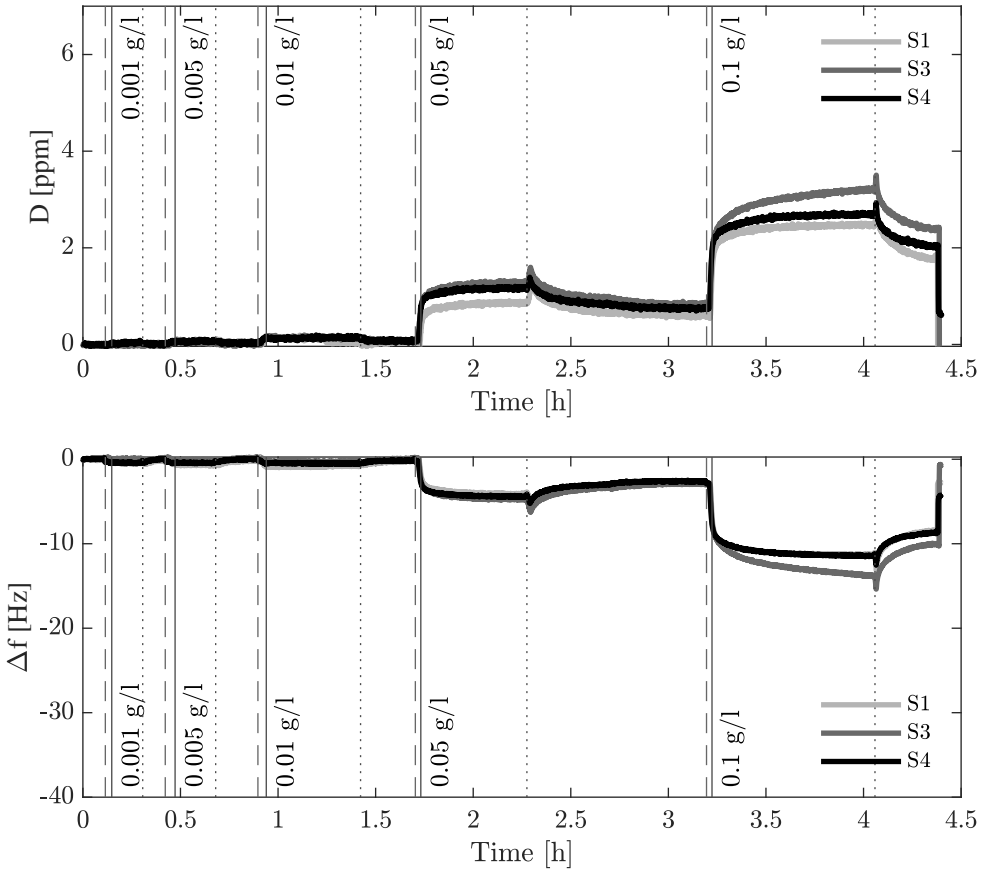

Figure 4.10 – Shows dissipation (upper) and frequency shift (lower) at third overtone for GGM using a PSU-coated sensor. Dashed lines mark pumping of new concentration, solid line marks beginning of adsorption period, dotted line marks the end of the adsorption period followed by flushing with water.

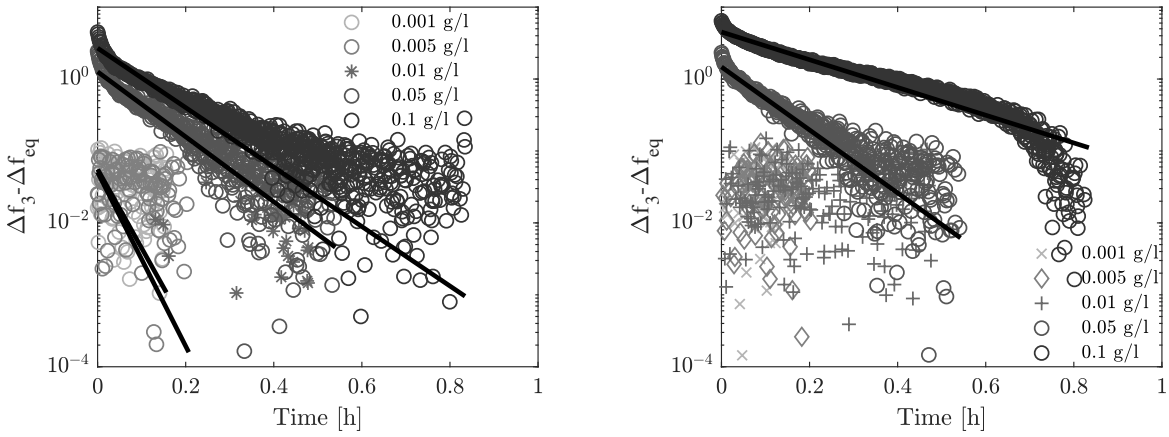

Figure 4.11 – Difference in frequency shift between time and equilibrium for sensor 1(S1, upper left) and sensor 3 (S3, upper right). Time is from the beginning of each concentration. Solid lines are least-square root fit for each concentration. For concentrations without solid lines, a least-square root fit could not be found. Note: Negative values are not shown.

The decay constants for each concentration and experiment with GGM on PSU are shown in Figure 4.12. As in the experiments with GGM on gold, these results do not show the linear dependence on initial bulk concentration as described in Section 2.3.1.

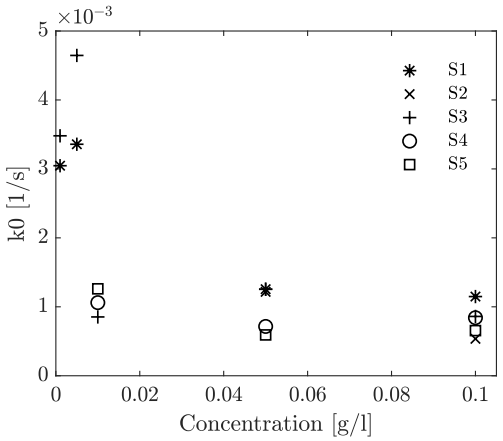

Figure 4.12 – Decay constants, k_0, for GGM on PSU at different initial bulk concentrations.

4.2 Simulation results

This section presents the results for the simulations done in COMSOL Multiphysics® (COMSOL AB, Sweden). First it presents the simulation of the flow in then sensor chamber without adsorption, then the simulation of the reference system and finally the simulation results for GGM on gold.

4.2.1 Flow simulations

The Laminar Flow physic models the flow within the sensor chamber. Figure 4.13 shows the velocity profile within the chamber at an inflow of 0.2 mL/min. At the centre point between the inlet and outlet and at 0.23 mm above the sensor surface, the velocity is 1.49 mm/s a slightly higher flow rate along the axis between the inlet and the outlet.

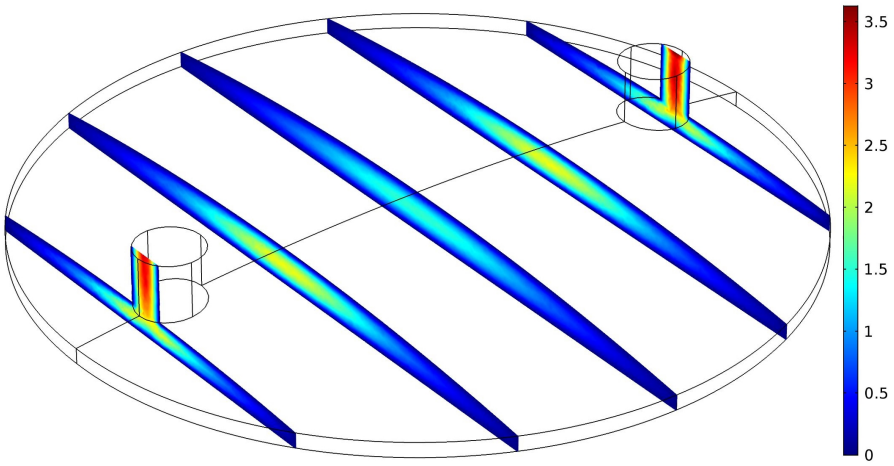

Figure 4.13 – Velocity profile in the sensor chamber in mm/s for an inlet volume flow of 0.2 mL/min not

Figure 4.14 shows how the average concentration changes in the bulk and at the outlet when a new solution is pumped into a water-filled sensor chamber. The example given is for GGM at 6 concentrations from 0.0001 g/L to 0.1 g/L at a flow rate of 0.2 mL/min and 90 % of inlet concentration is reached in the bulk after 50 seconds. However, this only considers an 1 mm long inlet and not the internal path to preheat the liquid nor any tubing from the sample holder to the unit.

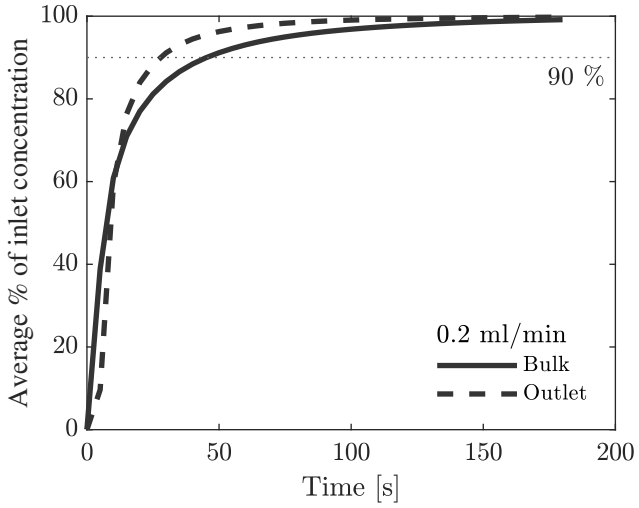

Figure 4.14 – Average bulk concentration (solid) and outlet concentration (dashed) in percentages of inlet concentration when pumping a solution of 0.1 g/L GGM into a sensor chamber filled with water during 3 minutes.

4.2.2 Simulation of the reference system

The reference model was built based on the adsorption parameters presented by Wu et al. (2007) (see Section 2.3.1) and the description of diffusivity as described in Section 3.3.3. The maximum possible concentration of adsorption sites, Γ_s, was estimated based on the equilibrium surface concentrations provided by Wu et al. (2007). Figure 4.15 shows the frequency shift of PNIPAM and two models of the Langmuir isotherm, Equation 2.8 fitted to the data. One model is fitted allowing the least square fit to modify both the Γ_s and the K to fit the model to the data. The other only allowed modification of Γ_s and fixing K to the ratio of k_{ads}/k_{des}=432 wt%$^{-1}$. The 2-parameter fit shows a better fit to the data point and gave a Γ_s of 173 Hz or 4.34×10^{-7} mol/m^2 and a K of 1633 wt%$^{-1}$. The 1-parameter fit has a worse fit to the data and gave a Γ_s of 246 Hz or 6.16×10^{-7} mol/m^2. Parameters for the reference model are summarised in Table 4.1

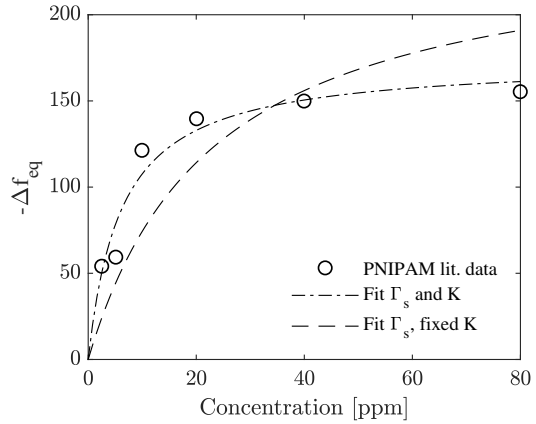

Figure 4.15 – Γ_s and K (dot-dashed) and Γ_s and K=432 wt%$^{-1}$ (dashed) fitted to literature data for equilibrium frequency shift Δf_{eq} for PNIPAM.

Table 4.1 – Reference model parameters

Parameter	Symbol	Value
Molar weight of PNIPAM	M_{PNIPAM}	23 574 g/mol
Adsorption coefficient	k_{ads}	152.2 L/(mol s)
Desorption coefficient	k_{des}	1.74×10^{-4} 1/s
Maximum concentration of adsorption cites	Γ_s	4.34×10^{-7} mol/m^2
		or 6.16×10^{-7} mol/m^2

Figure 4.16, shows two 2-hour simulations of the reference system where the water-filled sensor chamber has an inflow of a solution with a given concentration at 0.2 mL/min during 3 minutes, simulating the pumping phase. Then the model is run for 2 hours, representing the adsorption phase. Figure 4.16a and 4.16c are modelled with a maximum concentration of adsorption sites of 4.34×10^{-7} mol/m^2 while Figure 4.16b and 4.16d are modelled with a maximum concentration of adsorption sites of 6.16×10^{-7} mol/m^2. Figure 4.16a and 4.16b show how the average bulk concentration changes with time. Figure 4.16c and 4.16d shows the frequency shift for the third overtone that corresponds to the adsorbed mass according to the Sauerbrey relationship, Equation 2.1.

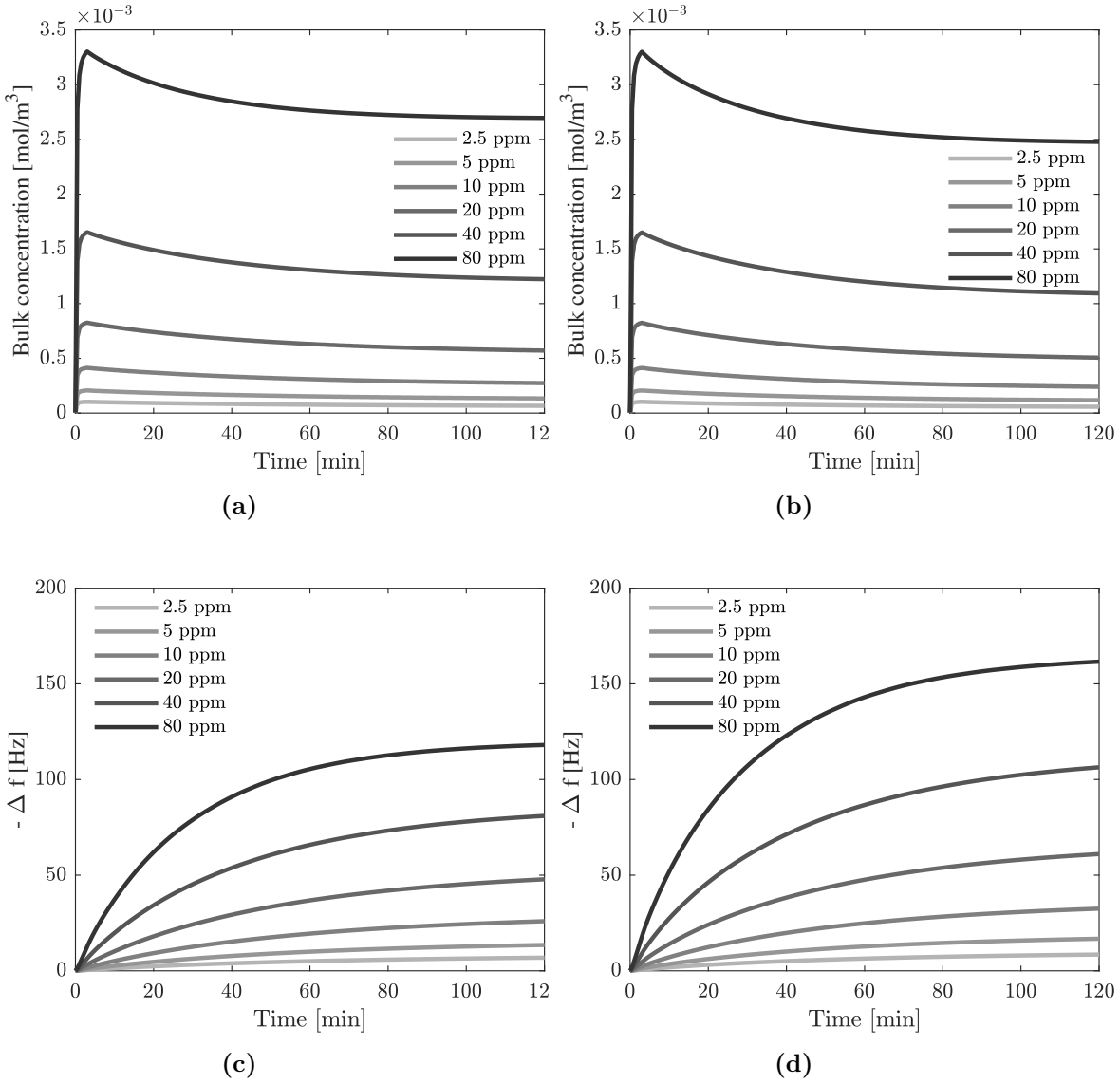

Figure 4.16 – Simulation of bulk concentration and corresponding frequency shift to simulated adsorbed mass for Γ_s=4.34 × 10^{-7} mol/m^2 and Γ_s=6.16 × 10^{-7} mol/m^2.

4.2.3 Simulation of GGM on Gold

The kinetic model that could be fitted the best to the data for GGM was the pseudo-second-order model (Section 4.1.3). However, the pseudo-second-order model did not integrate well into COMSOL. The model, for all concentrations and both time-dependent and steady-state modelling, resulted in a negative average bulk concentration, which is not physically possible. For the time-dependent modelling, the negative average bulk-concentration occurred immediately both for simulation starting with the initial concentration in the bulk or when pumped in. When setting the k_2- and q_e-expressions as variables dependent on the variable of local bulk concentration, c_A, it caused an error in the solver.

5 Discussion

5.1 Adsorption studies

The three substances glucose, dextran and GGM had very different interactions with the sensors. Glucose showed barely any tendency to adsorb, see Figure A.1 in Appendix, even at 0.15 g/l the frequency shift was very small. The frequency dissipation shift observed at 0.15 g/l is probably caused by the change in the density and viscosity of the bulk solution due to the increased sugar concentration, rather than adsorption.

In contrast to glucose, dextran showed stronger adsorption kinetics than glucose. However, on PSU the frequency shift did not seem to increase with an increased concentration, see Figure 4.2. Dextran on gold showed an increased frequency shift with an increased concentration but the frequency shift stopped once the pump was turned off. This indicates that the adsorption did not continue once the flow of dextran stopped. The difference in frequency shift between Sensor 1 and Sensor 4 when pumping 0.17 g/L dextran remains unclear. It could be differences in pump efficiency between the different flow channels caused by the tubing that the pump acts upon being more or less worn. If this is the case, this experiment might yield a clearer result if the pump and tubing are checked to guarantee proper performance. The larger frequency shift could also be a jump in the baseline similar to that of glucose. Neither explanation justifies why the adsorption of dextran would stop when the pump is stopped.

Compared to glucose and dextran, GGM shows strong adsorption kinetics onto both PSU and gold with a larger frequency shift for gold. For GGM on gold, there was an increasing difference in frequency shift between sensor 1 and sensor 2. This was probably caused by one of the sensors reaching a higher bulk concentration. During the experiments, it was observed that Sensor 2 reacted to the new concentration a few seconds earlier than Sensor 1. This delay could either be due to a small difference in length for the tubing between the sensors and the sample vial or a difference in pump efficiency due to worn tubing, as discussed for dextran.

When fitting the Langmuir model to the data, both GGM on gold and on PSU showed an exponential decrease in the decay constant k_0 with increased concentration and were in the same order of magnitude. This is, as mentioned before, not in line with the theory outlined in Section 2.3.1. For the lower concentrations the high decay constant could be caused by using too many data points when the experiment was already at equilibrium. This is something that can introduce errors in the adsorption model parameters (Cherkasov, 2020). The lower concentrations had shorter measurement time, thus making the last five minutes, when the equilibrium frequency shift was calculated, a relatively larger part of the data set. However, this does not explain why the decay constant was fairly constant for the higher concentrations. This is an indicator that GGM onto PSU and gold might not follow Langmuir adsorption kinetics. The basic assumptions for the Langmuir adsorption kinetics imply that the coefficients for adsorption and desorption are independent of the concentration of the adsorbed substance and the concentration in the bulk. If the decay constant, $k_{0,}$ in Equation 2.11 does not change with the concentration, the other parameters k_a and k_d must change instead.

Fitting the Langmuir model to the data for adsorption of GGM on gold and on PSU is also based on the assumption that the Sauerbrey relationship is valid. At least for GGM on gold, the assumption is not valid, as mentioned in Section 4.1.3, due to the large change in dissipation compared with the frequency shift. GGM on PSU shows both a smaller frequency shift and change in dissipation than GGM on gold. However the relative change in dissipation relative to the frequency shift is still pretty big and a reason to doubt the validity of using Sauerbrey. This introduces additional errors to the parameters.

For the pseudo-first-order model, it is clear that it is not a good fit to data for GGM on gold when fitted with the linearised form of the expression (Section 4.1.3). The pseudo-first-order model is commonly best fitted to the early parts of the adsorption process. It is not unreasonable to assume that the pseudo-first-order model could be fitted to the initial part of the GGM adsorption as the curve is steeper at the initial part of the measurement period (Figure 4.7). Opposed to the pseudo-first-order model, the pseudo-second-order model showed a very good fit to the data points, with a coefficient of determination over 0.97 for all concentrations except 0.0001/L for one sensor where it was 0.72. However, the pseudo-second-order model might fit better due to mathematical reasons rather than physical reasons (Section 2.3.2).

An issue with the pseudo-order-models is that they have no parameter defining the desorption of the adsorption/desorption process, as the Langmuir model does. They also do not have an apparent connection with the bulk concentration, which is an challenge since there needs to be an adsorbable substance in the bulk for adsorption to occur. To make the parameters in the rate expression depend on the initial bulk concentration is a very crude method to try to adapt the pseudo-order-models to a range of concentrations.

The chosen method to investigate the adsorption kinetics might not be a suitable method for the reasons given by Cherkasov (2020). The study has not considered the effects of the bulk solution on the surface and subsequent response in the QCM-D measurement. The fundamental assumptions for Langmuir kinetics might not apply, making it an unsuitable model to fit the parameters. For the pseudo-first-order and pseudo-second-order, the adsorption models were fitted to the data created by one solution to the Voigt model in Dfind. This this approach introduces additional errors to the kinetics parameters. As can be seen in Figure 4.6, there is a large difference between the two solutions of the Smartfit model and the choice of which model to proceed with has a great effect on the parameters as well.

5.2 Flow simulations

The flow simulations showing the change in bulk and outlet concentration, Figure 4.14, shows that it takes 50 s for the bulk of the sensor cell to reach 90 % of the inlet solution. There is an additional delay of the tubing of approximately 40 s and of the internal channel before the sensor of maximum 30 s. Thus, 90 % of the initial concentration is reached between 90 s to 120 s after the pump is started. Stopping the pump too early would result in a large underestimation of the bulk concentration. If the tubing length is different before the different sensors this would cause them to have different real bulk concentrations too. This is an issue for all the measurements as the true initial concentration above the sensor remains unknown. This introduces further errors to the fitted parameters. Especially when studying the adsorption isotherm it is important to know the equilibrium concentration for the bulk and the surface. The initial bulk concentration could function as a rough approximation since it is not possible to measure the bulk concentration in the

setup used. Calculating the bulk concentration at the equilibrium by subtracting the adsorbed mass from the initial bulk concentration is also a rough approximation as it will contain the error of the initial bulk concentration and any error in the use of Saurebrey or Voigt models to estimate the adsorbed mass.

5.3 Reference model simulations

For the reference model simulations the higher estimate for maximum surface concentration of adsorption sites, Γ_s, gave consistently higher surface concentrations than the lower estimates. However, only the higher estimate at an inlet concentration of 80 ppm gave simulated frequency shift close the equilibrium frequency shift given by Wu et al. (2007). There are several reasons why the simulated results do not match the data that it is based on. The mass sensitivity coefficient in the Sauerbrey relationship used might not be the same as in the experiment since the value of the constant was not stated. This error can give the wrong maximum concentration of adsorption sites and therefore either overestimate or underestimate the rate of adsorption. The model is also based on the assumption that both the Langmuir kinetic model and the Sauerbrey relationship are valid for the system. In the article by Wu et al. (2007), the small difference in frequency shift between 2.5 ppm and 5 ppm as explained with the completion of the monolayer and that the continued adsorption is through densification of the layer. The completion of the monolayer means that the Langmuir isotherm, which was used to estimate the maximum concentration of adsorption sites is no longer valid. The densification of the layer means that less solvent is affecting the sensor per molecule adsorbed. This would overestimate the mass adsorbed at low concentrations and underestimate the adsorption at high concentrations.

5.4 GGM-model simulation

The method to fit the Langmuir model to the data did not match for neither GGM on gold nor GMM on PSU, only the pseudo-second-order model was integrated with COMSOL. However, the pseudo-second-order adsorption kinetics was not properly integrated with the COMSOL model and as a result, the simulation results showed negative bulk concentrations. The key issue is the lack of connection between bulk

concentration and the adsorption rate. In the used model the parameters k_2 and q_e are fixed values determined by the inlet concentration. The concentration of the adsorbed substance, c_s, is the only variable that changes over time. This means that no consideration is taken to the concentration of the unadsorbed substance in the immediate surrounding of the surface. In reality, the concentration in the immediate surrounding of the adsorption site heavily affects the adsorption rate: if no adsorbate is present, nothing can adsorb and the rate will be zero. The attempt to make q_e and k_2 dependent on the local bulk concentration, c_A, did not work due to the expression chosen to describe k_2, $y = a \cdot x^b$. When b is negative the expression grows towards infinity when x, the concentration, goes toward 0. This shows the risk of selecting empirical equations providing the best fit without considering whether they reflect the physical reality.

One issue with the COMSOL model, which applies both to the reference model and the GGM-model, is how to interpret and compare the simulation results with the experimental data. As long as the Sauerbrey relationship is valid, it is possible to convert surface concentration (output from the COMSOL model) to frequency shift (the result for the QCM-D measurement). However, if the Sauerbrey relationship is not valid, then there is no obvious way for the current COMSOL model to be compared to the experimental data. The COMSOL model does not simulate the viscoelastic properties of the adsorbed layer and thus there is no way to compare the dissipation of the experimental data with the model. The layer modelling done by Dfind could be compared with surface concentration simulated by COMSOL but that would be affected by the choice of layer model as discussed in Section 5.1.

6 Conclusion

The aim of this project was to model the adsorption process of hemicellulose onto a model membrane surface. No strong adsorption kinetics could be observed for the model compounds glucose and dextran. GMM showed strong adsorption kinetics on both PSU and gold surface. However, the Langmuir kinetic model could not be fitted to the experimental data as planned. Attempting to fit the pseudo-order adsorption models to the adsorption of GGM on gold showed that the pseudo-second-order model had a good fit but the pseudo-first-order model did not. The attempt to simulate the pseudo-second-order in COMSOL failed due to the lack of suitable coupling of the bulk concentration with the adsorption kinetics.

The reference model for the COMSOL simulation functioned. However, when comparing the simulation results with the literature data it did not match. This could be attributed to the validity of the Langmuir isotherm and kinetics and the method to compare the simulation results with the data.

The flow simulations highlighted the issue of dilution of the bulk concentration when a higher concentration is pumped into the cell. This is something that must be considered when designing future experiments.

If it is desirable to continue the project of simulating the adsorption process of hemicellulose a more rigorous investigation of the adsorption process must be done. Only measuring the adsorption with QCM-D might not be sufficient. The choice of model for the adsorption kinetics to evaluate the data must be considered as well as how it is integrated into COMSOL.

7 Future Work

To be able to simulate adsorption of hemicellulose onto the model surface of a QCM-D sensor there are several things that can be improved.

Most importantly a rigorous study, as discussed by Cherkasov (2020), on the adsorption kinetics and isotherm must be performed. The set up for the experiment must be considered and whether QCM-D is a suitable method to perform the measurements. Combining QCM-D with a mass-sensitive optical technique could be an option to mitigate the effects of the solvent. One could also consider running the adsorption study continuously since then it is reasonable to assume that the bulk concentration is the same as the inlet concentration. Other kinetic models and adsorption isotherms should be investigated to see if they are applicable. Diffusivity for GGM should be determined experimentally and the validity of neglecting the surface diffusion should also be investigated. If the adsorption kinetics can be successfully determined the next step is to investigate the temperature dependence of the adsorption and diffusion.

For the simulations, care must be taken to ensure that the adsorption kinetics can be integrated properly. Other things that should be considered are the mesh size and geometry for the calculations, which have not been discussed in this project. A way to evaluate the simulation results for the adsorption must be established for cases when the Saurebrey relationship does not apply.

References

Alfa Laval (2020). *Alfa Laval UF flat sheet membranes*. URL: https://www.alfalaval.com/products/separation/membranes/flat-sheet-membranes/uf-flat-sheet/ (visited on 06/07/2020).

Alveteg, Mattias, ed. (2020). *Handbook - Physical properties, correlations and equations*. 2020th ed. Department of Chemical Engineering, Faculty of Engineering, Lund University: Lund.

Atkins, P W and Julio De Paula (2010). *Atkins' physical chemistry*. Oxford University Press: Oxford, New York, pp. 885–891. ISBN: 9780199543373 (hft.)

Biolin Scientific, Sweden (2019). *QSense Analyzer Operator Manual*. Ed. by Ilkka Hokajärvi.

Biolin Scientific, Sweden (2020). *Instruments and Accessories FAQ — QSense — Support Portal*. URL: https://www.biolinscientific.com/support-portal/qsense/academy/faq-instruments-and-accessories%7B%5C#%7Dwhat-is-the-reynolds-numbers-for-the-flow-module (visited on 02/12/2020).

Biolin Scientific, Sweden (n.d.). *Quartz Crystal Microbalance with Dissipation (QCM-D)*. Tech. rep.

Bokhary, A. et al. (June 2017). "A review of membrane technologies for integrated forest biorefnery". In: *Journal of Membrane Science and Research* 3(3), pp. 120–141. ISSN: 24765406. DOI: 10.22079/jmsr.2016.22839.

Caligur, Vicki (2008). *Dextran and Related Polysaccharides*. Tech. rep. URL: https://www.sigmaaldrich.com/technical-documents/articles/biofiles/dextran-and-related.html.

Cherkasov, Nikolay (2020). "Liquid-phase adsorption: Common problems and how we could do better". In: *Journal of Molecular Liquids* 301, p. 112378. ISSN: 01677322. DOI: 10.1016/j.molliq.2019.112378. URL: https://doi.org/10.1016/j.molliq.2019.112378.

Comsol (n.d.). *Transport and Adsorption - Comsol 5.3a*. Tech. rep. URL: https://www.comsol.se/model/transport-and-adsorption-5.

Dal-Cin, M M et al. (1996). "Membrane performance with a pulp mill effluent: Relative contributions of fouling mechanisms 1". In: *Journal of Membrane Science* 120, pp. 273–285. DOI: https://doi.org/10.1016/0376-7388(96)00151-2.

Ding, Zhaodong et al. (Oct. 2016). "Enhancing the compatibility, hydrophilicity and mechanical properties of polysulfone ultrafiltration membranes with lignocellulose nanofibrils". In: *Polymers* 8(10). ISSN: 20734360. DOI: 10.3390/polym8100349.

Hansen, Natanya M.L. and David Plackett (2008). *Sustainable films and coatings from hemicelluloses: A review*. DOI: 10.1021/bm800053z.

Hartman, Jonas et al. (2006). "Oxygen barrier materials from renewable sources: Material properties of softwood hemicellulose-based films". In: *Journal of Applied Polymer Science* 100(4), pp. 2985–2991. ISSN: 00218995. DOI: 10.1002/app.22958.

He, Kan et al. (2018). "Molecular weight determination of Aloe polysaccharides using size exclusion chromatography coupled with multi-angle laser light scattering and refractive index detectors". In: *Journal of AOAC International* 101(6), pp. 1729–1740. ISSN: 10603271. DOI: 10.5740/jaoacint.18-0121.

Jönsson, Ann-Sofi (Jan. 2013). "Microfiltration, Ultrafiltration and Diafiltration". In: *Separation and Purification Technologies in Biorefineries*. Ed. by Shri Ramaswamy, Hua-Jiang Huang, and Bandaru V. Ramarao. wiley: Chichester, UK, pp. 205–231. ISBN: 9781118493441. DOI: 10.1002/9781118493441.ch8. URL: http://doi.wiley.com/10.1002/9781118493441.ch8.

Lindblad, Margaretha Söderqvist et al. (2005). "Biodegradable polymers from renewable sources: Rheological characterization of hemicellulose-based hydrogels". In: *Biomacromolecules* 6(2), pp. 684–690. ISSN: 15257797. DOI: 10.1021/bm049515z. URL: https://pubs.acs.org/sharingguidelines.

Liu, Guangming and Guangzhao Zhang (2013). "Basic Principles of QCM-D". In: *QCM-D Studies on Polymer Behavior at Interfaces*. Springer, Berlin, Heidelberg: Berlin, Heidelberg. Chap. 1, pp. 1–8. ISBN: 978-3-642-39790-5. DOI: 10.1007/978-3-642-39790-5_1. URL: https://doi.org/10.1007/978-3-642-39790-5%7B%5C_%7D1.

Lundqvist, Jon et al. (2002). "Isolation and characterization of galactoglucomannan from spruce (Picea abies)". In: *Carbohydrate Polymers* 48(1), pp. 29–39. ISSN: 01448617. DOI: 10.1016/S0144-8617(01)00210-7. URL: www.elsevier.com/locate/carbpol.

Moussout, Hamou et al. (June 2018). "Critical of linear and nonlinear equations of pseudo-first order and pseudo-second order kinetic models". In: *Karbala International Journal of Modern Science* 4(2), pp. 244–254. ISSN: 24056103. DOI: 10.1016/j.kijoms.2018.04.001.

Nilsson, Bernt and Niklas Andersson (2018). *Applied Transport Phenomena: Course slides*. November. Lund.

Pérez Nebreda, A. et al. (Feb. 2019). "Modelling of homogeneously catalyzed hemicelluloses hydrolysis in a laminar-flow reactor". In: *Chemical Engineering Science* 195, pp. 758–766. ISSN: 00092509. DOI: 10.1016/j.ces.2018.10.021.

Persson, T. et al. (June 2010). "Fractionation of process water in thermomechanical pulp mills". In: *Bioresource Technology* 101(11), pp. 3884–3892. ISSN: 09608524. DOI: 10.1016/j.biortech.2009.12.142.

Qiu, Hui et al. (2009). *Critical review in adsorption kinetic models*. DOI: 10.1631/jzus.A0820524. URL: www.zju.edu.cn/jzus;.

Qsense Biolin Scientific (2020). *QCM-D — Measurements*. URL: https://www.biolinscientific.com/measurements/qcm-d (visited on 06/03/2020).

Qsense Biolin Scientific, Sweden (n.d.). *Dfind Help & Manual*.

Ragnar, Martin et al. (May 2014). "Pulp". In: *Ullmann's Encyclopedia of Industrial Chemistry*. Wiley-VCH Verlag GmbH & Co. KGaA: Weinheim, Germany, pp. 1–

92. DOI: 10.1002/14356007.a18_545.pub4. URL: http://doi.wiley.com/10.1002/14356007.a18%7B%5C_%7D545.pub4.

Reviakine, Ilya, Diethelm Johannsmann, and Ralf P Richter (2011). "Hearing What You Cannot See and Visualizing What You Hear: Interpreting Quartz Crystal Microbalance Data from Solvated Interfaces". In: *Anal. Chem* 83, pp. 8838–8848. DOI: 10.1021/ac201778h.

Al-Rudainy, Basel, Mats Galbe, and Ola Wallberg (Oct. 2017). "Influence of prefiltration on membrane performance during isolation of lignin-carbohydrate complexes from spent sulfite liquor". In: *Separation and Purification Technology* 187, pp. 380–388. ISSN: 18733794. DOI: 10.1016/j.seppur.2017.06.031.

Rudolph, Gregor et al. (2019). "A review of in situ real-time monitoring techniques for membrane fouling in the biotechnology, biorefinery and food sectors". In: *Journal of Membrane Science* 588, p. 117221. ISSN: 0376-7388. DOI: https://doi.org/10.1016/j.memsci.2019.117221. URL: http://www.sciencedirect.com/science/article/pii/S0376738819310531.

Schenck, Fred W. (Dec. 2006). "Glucose and Glucose-Containing Syrups". In: *Ullmann's Encyclopedia of Industrial Chemistry*. Wiley-VCH Verlag GmbH & Co. KGaA: Weinheim, Germany. DOI: 10.1002/14356007.a12_457.pub2. URL: http://doi.wiley.com/10.1002/14356007.a12%7B%5C_%7D457.pub2.

Schmitt, Uwe, Gerald Koch, and Ralph Lehnen (Jan. 2014). "Wood". In: *Ullmann's Encyclopedia of Industrial Chemistry*. Wiley-VCH Verlag GmbH & Co. KGaA: Weinheim, Germany, pp. 1–18. DOI: 10.1002/14356007.a28_305.pub2. URL: http://doi.wiley.com/10.1002/14356007.a28%7B%5C_%7D305.pub2.

Sörensson, Robert and Anders Jonsson (2014). *Företag inom svensk massa-och pappersindustri*. Tech. rep. URL: www.VINNOVA.se..

Thuvander, Johan and Ann Sofi Jönsson (2016). "Extraction of galactoglucomannan from thermomechanical pulp mill process water by microfiltration and ultrafiltration-Influence of microfiltration membrane pore size on ultrafiltration performance". In: *Chemical Engineering Research and Design* 105, pp. 171–176. ISSN: 02638762. DOI: 10.1016/j.cherd.2015.12.003. URL: http://dx.doi.org/10.1016/j.cherd.2015.12.003.

Thuvander, Johan, Frank Lipnizki, and Ann-Sofi Jönsson (May 2019). "On-Site Recovery of Hemicelluloses from Thermomechanical Pulp Mill Process Water by Microfiltration and Ultrafiltration". In: *Journal of Wood Chemistry and Technology* 39(3), pp. 214–223. ISSN: 0277-3813. DOI: 10.1080/02773813.2019.1565865. URL: https://www.tandfonline.com/doi/full/10.1080/02773813.2019.1565865.

Timell, Tore E. (1967). "Recent progress in the chemistry of wood hemicelluloses". In: *Wood Science and Technology* 1(1), pp. 45–70. ISSN: 00437719. DOI: 10.1007/BF00592255.

Tremblay, Andre Y, Chung M Tam, and Michael D Guiver (1992). "Variations in the Pore Size of Charged and Noncharged Hydrophilic Polysulfone Membranes". In: *Industrial and Engineering Chemistry Research* 31(3), pp. 834–838. ISSN:

15205045. DOI: 10.1021/ie00003a027. URL: https://pubs.acs.org/sharingguidelines.

Willför, S. et al. (May 2003). "Characterisation of water-soluble galactoglucomannans from Norway spruce wood and thermomechanical pulp". In: *Carbohydrate Polymers* 52(2), pp. 175–187. ISSN: 01448617. DOI: 10.1016/S0144-8617(02)00288-6.

Wu, Bing et al. (Jan. 2007). "Adsorption kinetics and adsorption isotherm of poly(N-isopropylacrylamide) on gold surfaces studied using QCM-D". In: *Journal of Physical Chemistry C* 111(3), pp. 1131–1135. ISSN: 19327447. DOI: 10.1021/jp066529l.

Yohannes, Gebrenegus et al. (Mar. 2005). "Characterisation of poly(N-isopropylacrylamide) by asymmetrical flow field-flow fractionation, dynamic light scattering, and size exclusion chromatography". In: *Journal of Separation Science* 28(5), pp. 435–442. ISSN: 1615-9306. DOI: 10.1002/jssc.200401880. URL: http://doi.wiley.com/10.1002/jssc.200401880.

Zasadowski, Dariusz et al. (2014). "Antisolvent precipitation of water-soluble hemicelluloses from TMP process water". In: *Carbohydrate Polymers* 113, pp. 411–419. ISSN: 01448617. DOI: 10.1016/j.carbpol.2014.07.033. URL: http://dx.doi.org/10.1016/j.carbpol.2014.07.033.

A Appendix 1

The frequency shift and dissipation for glucose on PSU-coated sensor are shown in figure A.1. Both sensors seem to be affected by a slight baseline drift. Their frequency shift seems to be slightly affected by the glucose at 0.15 g/l. This is probably due to the change in bulk density and viscosity.

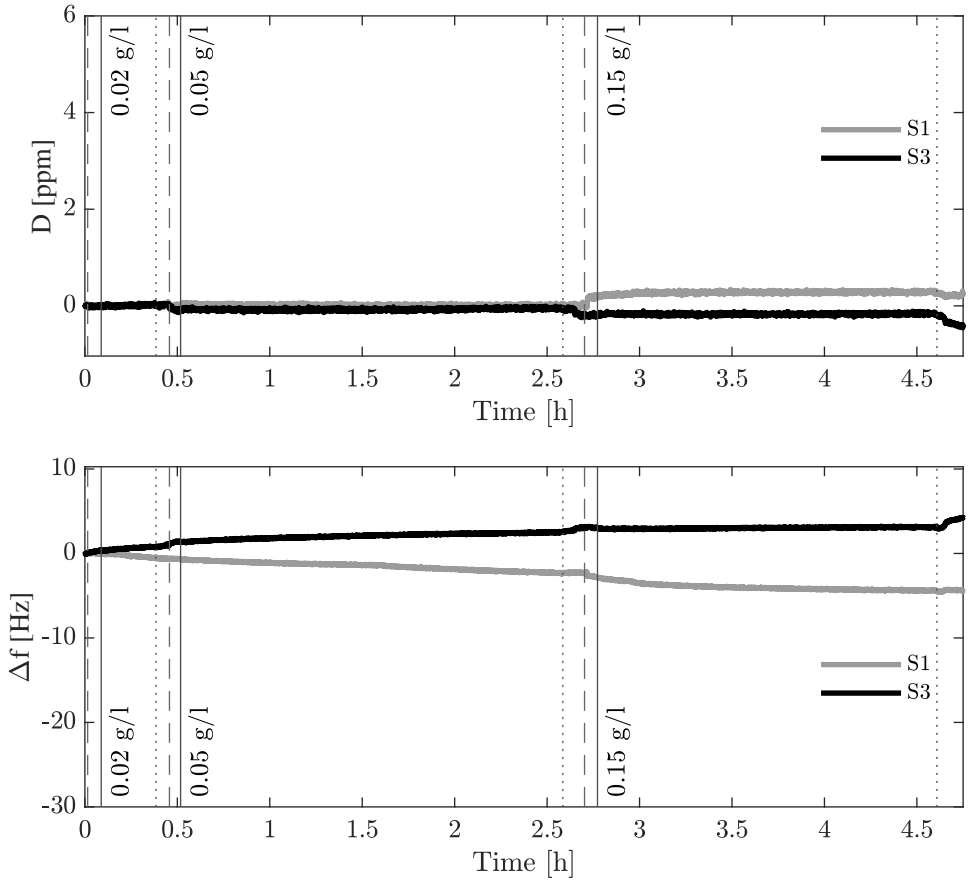

Figure A.1 – Dissipation (upper) and frequency shift (lower) for glucose on PSU at 0.02, 0.05 and 0.15 g/l. Dashed lines show when a new concentration is pumped into the cell, dotted lines show when the cell is flushed with water and solid lines show when the pump is turned off for each concentration.

B Appendix 2

Figure B.1 shows frequency shift and dissipation for the second experiment with GGM on PSU. The figure is comparable to Figure 4.10 in Section .

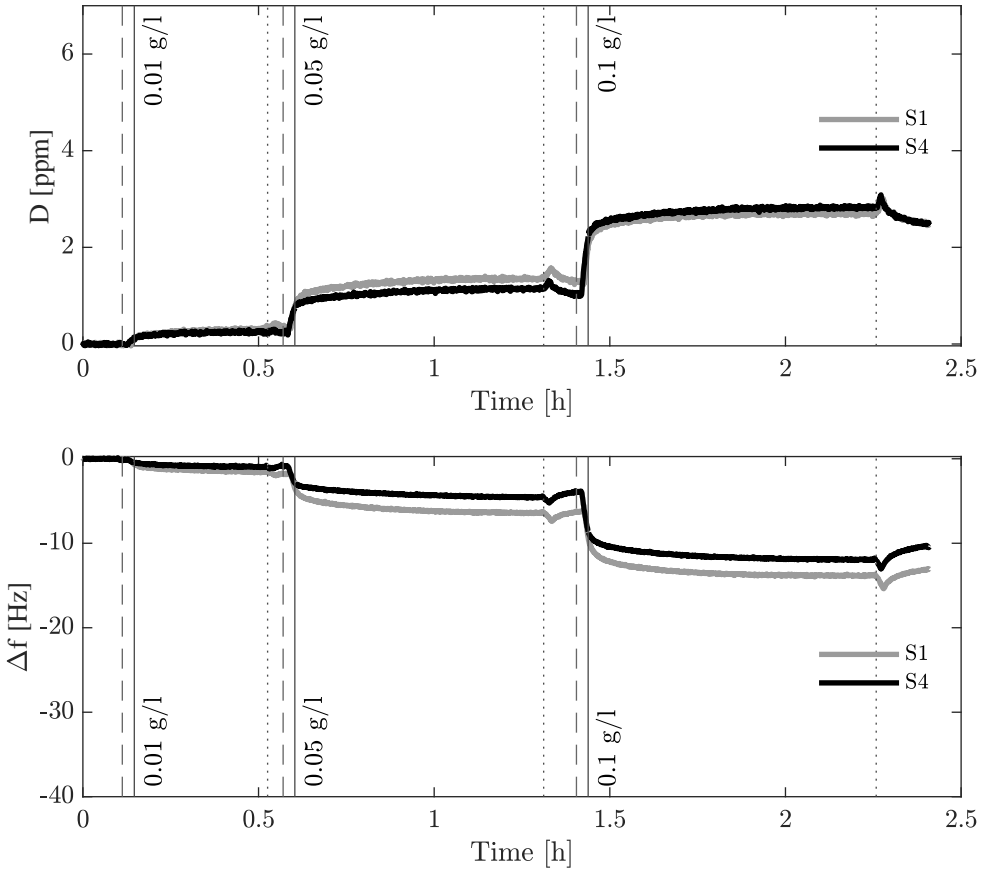

Figure B.1 – Shows dissipation (upper) and frequency shift (lower) at third overtone for GGM using a PSU-coated sensor. Dashed lines mark pumping of new concentration, solid line marks beginning of adsorption period, dotted line marks the end of the adsorption period followed by flushing with water.